Arab J Geosci (2015) 8:9237–9259
DOI 10.1007/s12517-015-1875-7

ORIGINAL PAPER

Integrated petrographic, mineralogical, and geochemical study of the Late Cretaceous–Early Tertiary Dakhla Shales, Quseir–Nile Valley Province, central Egypt: implications for source area weathering, provenance, and tectonic setting

Samir M. Zaid

Received: 17 September 2014 / Accepted: 1 March 2015 / Published online: 24 March 2015

Abstract Late Cretaceous–Early Tertiary shales of the Dakhla Formation of the Quseir–Qena Province, central Egypt, were analyzed for major and selected trace elements to infer their provenance, source rock paleoweathering intensity, and tectonic setting. The studied formation consists of a series of marls and shales and is subdivided into two members, namely Beida Shale Member at the top and Hamama Marl Member at the base. The Dakhla Shales are texturally classified as mudstones. Mineralogically, these shales consist mainly of smectite and kaolinite. Chemical analysis of the major and trace elements generally exhibits a uniform distribution throughout the Upper Maastrichtian–Lower Paleocene sediments. SiO_2, Al_2O_3, and Fe_2O_3 contents are higher than the values reported for the post-Archaean Australian shale (PAAS), while TiO_2 and Na_2O contents are found to be lower. Bivariate plot of Zr versus TiO_2 diagram indicates that intermediate to felsic igneous rocks constitute the main supplying source rock. Average chemical index of alteration (CIA), plagioclase index of alteration (PIA), and chemical index of weathering (CIW) values (81, 92, and 93 %, respectively) imply intermediate to intense weathering of the source material in a semiarid climate. The bivariate discriminant function diagram reveals an active continental to passive margin setting for the Dakhla Shales. The developed soils were transported by rivers to the depositional basin. The inferred tectonic setting for the Late Cretaceous–Early Tertiary Dakhla Shales in Quseir–Qena Province is in agreement with the tectonic evolutionary history of central Egypt during the Late Cretaceous–Early Tertiary.

Keywords Provenance · Dakhla Shales · Central Egypt

S. M. Zaid (✉)
Geology Department, Faculty of Sciences, Zagazig University, Zagazig 44511, Egypt
e-mail: samir_zaid75@yahoo.com

Introduction

Mineralogical and chemical characteristics of mudrocks are controlled by various factors including the composition of their source rocks, the extent of weathering, mode of transportation, and post-depositional processes (Taylor and McLennan 1985; Hayashi et al. 1997). However, the tectonic setting of the sedimentary basin may play a predominant part over other factors because different tectonic settings can provide different kinds of source materials with variable chemical signatures (e.g., Bhatia 1983; Bhatia and Crook 1986; Roser and Korsch 1986; McLennan et al. 1993; Nesbitt et al. 1997; Cullers 2000; Purevjav and Roser 2012; Yan et al. 2012). Many attempts have been made to refine provenance models using geochemical features (e.g., Bhatia 1983; Suttner and Dutta 1986; Roser and Korsch 1986, 1988; Armstrong-Altrin et al. 2004, 2012, 2013, 2014; Zaid 2012, 2013, 2015).

Due to its fine-grained nature and impermeability, mudrocks retain most of the mineral constituents of the source rocks (Blatt 1985; Graver and Scott 1995). The bulk geochemistry of shales, thus, preserves the near-original signatures of the provenance and more faithfully reflects paleoweathering conditions and diagenetic history much better than any other siliciclastic rocks.

Major oxides (e.g., TiO_2 and Al_2O_3) are particularly useful for provenance interpretations. Being immobile phases in aqueous systems, these oxides retain the original source rock concentration within the shales (Hayashi et al. 1997). Besides the major oxides, the concentration of trace elements is also used to characterize provenance in shales. For example, the abundance of zirconium, vanadium, nickel, and barium in shales provides significant information about the nature of source rocks (Nesbitt and Young 1984, 1989; Roser and Korsch 1986; Fedo et al. 1995, 1996; Sugitani et al. 1996; Hayashi et al. 1997; Moosavirad et al. 2011; Armstrong-Altrin et al. 2013, 2015).

The Dakhla Formation is of particular interest because of its rhythmic deposition of shale and glauconite-rich facies. Consequently, numerous studies have been published on the geology, stratigraphy, and sedimentology of the Maastrichtian–Lower Paleocene marine sediments exposed in central Nile Valley and Quseir District of the Eastern Desert (e.g., Said 1961; Issawi 1972; Faris 1984; Faris and Strougo 1998; Tantawy et al. 2001; Obaidalla et al. 2008; El-Azabi and Farouk 2010). However, studies related to mineralogy and geochemistry and their inferred provenance, weathering, and tectonic setting are meager.

The present work aims to reconstruct the provenance and tectonic setting of the Late Cretaceous–Early Tertiary Dakhla Formation shales, using an integrated approach involving modal analysis and bulk rock geochemistry data from three exposed sections: Gebel Atshan (Quseir District), Gebel Abu Had, and Gebel El Gir (central Nile Valley, Figs. 1 and 2).

Geological setting

The Late Cretaceous–Early Tertiary Dakhla Shale is widely distributed in Egypt and can be traced along the southern belt of the stable shelf from the Dakhla Oasis in the west through the Nile Valley to Quseir in the east (Said 1960; Issawi 1972). These shales outcrop on both sides of the Precambrian basement rocks that form the Red Sea Mountains. Shales have remarkably constant lithological characteristics and they form elongated, semiclosed basins within the dissected crystalline ridge.

The Cretaceous/Tertiary sequence in Quseir and Nile Valley areas is differentiated into several units, arranged from base to top: Nubia Sandstone, Quseir Variegated Shale, Duwi Formation, Dakhla Shale, Tarawan Chalk, Esna Shale, and Thebes Formation (Abdel Razik 1972). These sediments were deposited in the inner to middle shelf settings.

The Dakhla Formation (introduced by Said 1961) marks the Maastrichtian–Lower Paleocene sequence, conformably overlies the Duwi Formation, and is unconformably overlain by the Tarawan Chalk. This formation consists of intercalations of marls and shales and may reach a thickness of about 150–175 m. It is subdivided into two members, namely Beida Shale Member at the top and Hamama Marl Member at the base (Abdel Razik 1972). The lower member is about 75 m thick and consists of pink marls, in which planktonic foraminiferal assemblages yielded a Maastrichtian age (Abdel Razik 1972). The upper member is about 100 m thick and consists of gray to green shales, yellowish in some parts, and fissile with gypsum veinlets. This member is unconformably overlain by the Tarawan Chalk. The contact is marked by an abrupt change from gray shale with gypsum veinlets into brownish, reddish limestone and chalky white limestone. Abdel Razik (1972), Tantawy et al. (2001), Obaidalla et al. (2008), and

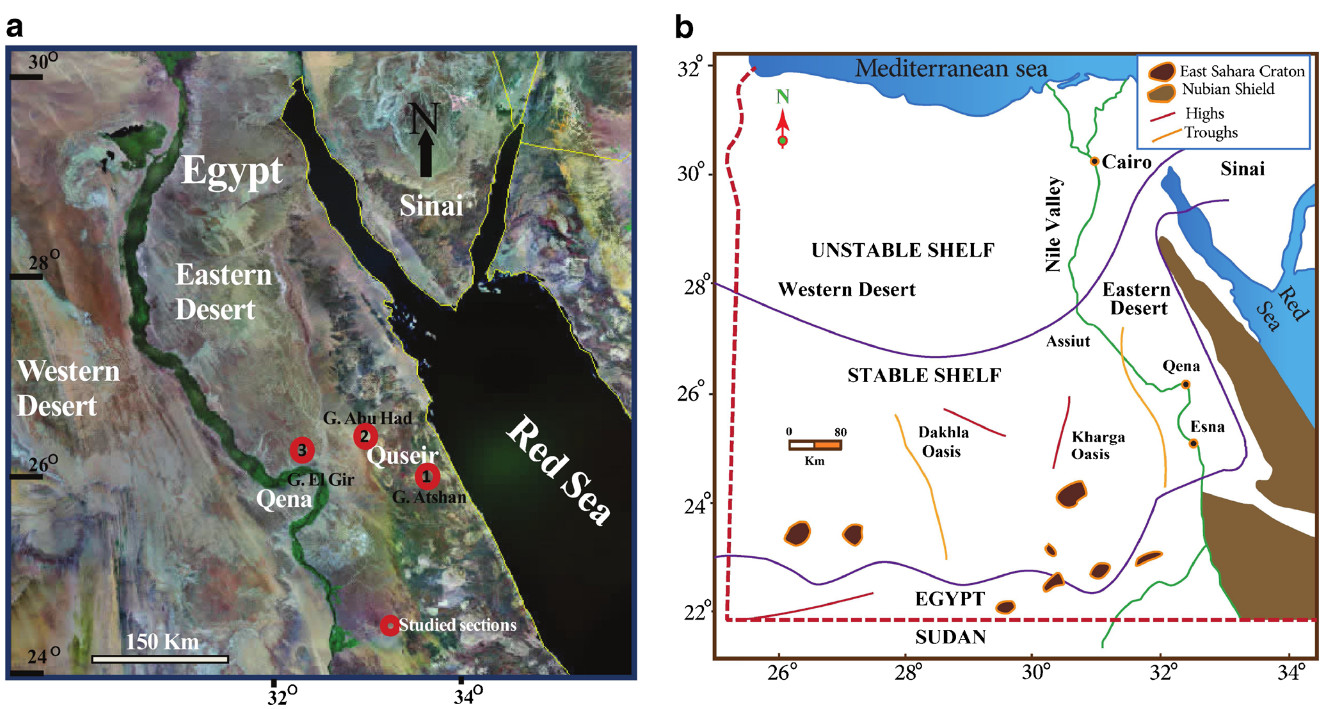

Fig. 1 Map showing the **a** location of the studied section and **b** major tectonic framework of Egypt (after Said 1962)

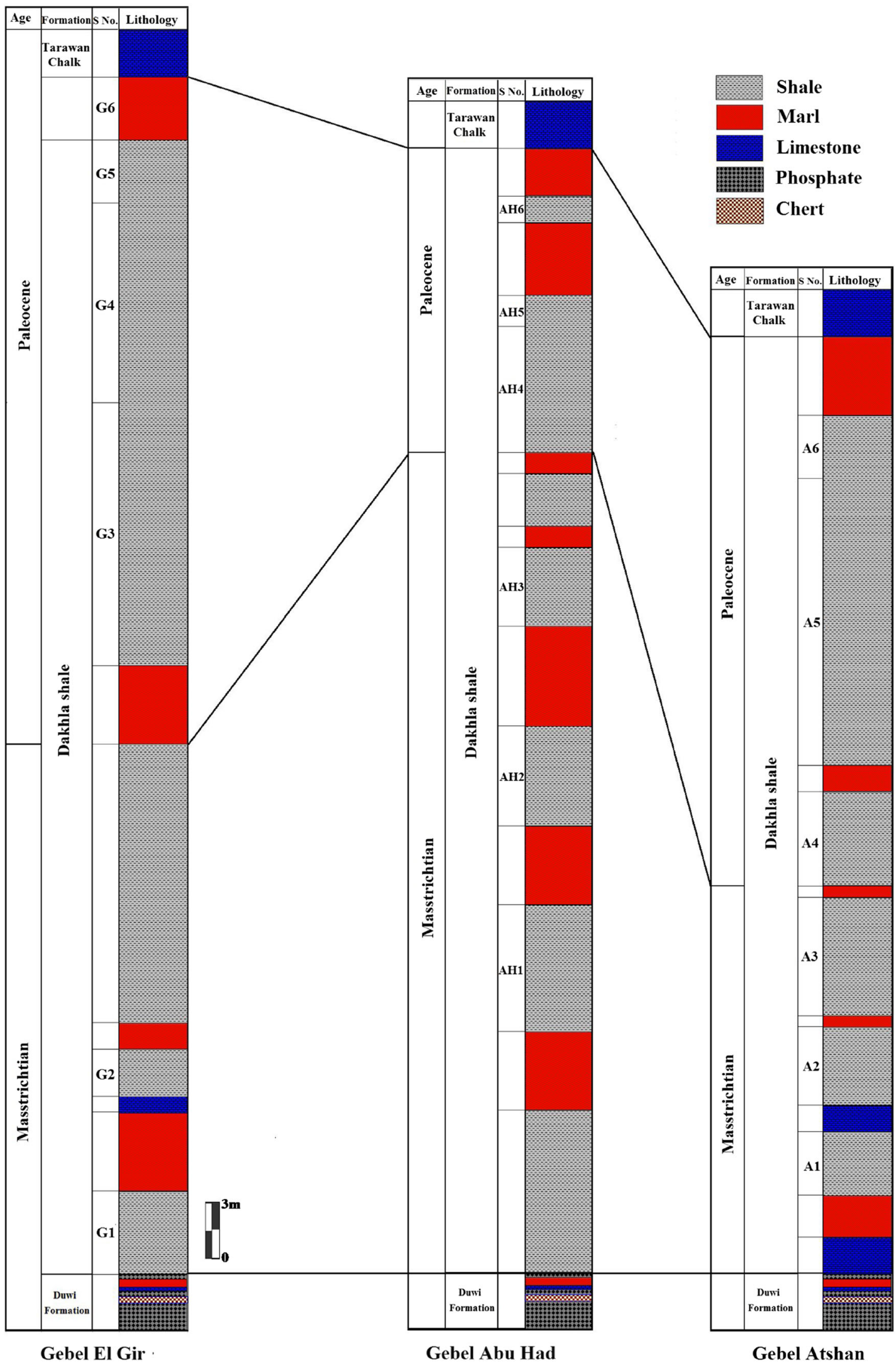

Fig. 2 Correlation chart of the Dakhla Formation at the studied locations: (1) G. Atshan, (2) G. Abu Had, and (3) G. El Gir, central Egypt

El-Azabi and Farouk (2010) emphasized that the Dakhla Formation was deposited under a predominantly marine environment with minor fluviatile condition influences.

Said (1962) subdivided Egypt into two major tectonic provinces, the tectonically deformed Unstable Shelf to the north (approximately to the north of latitude 28°) and the nearly horizontal and less deformed Stable Shelf to the south (Fig. 1b). Intracratonic sedimentary basins were developed on the southern Stable Shelf, whereas pericratonic or rift basins were formed on the northern Unstable Shelf (El Hawat 1997).

The Stable Shelf comprises the pre-rifting Cretaceous–Eocene sedimentary rock of the study area while the Unstable Shelf includes post-rifting Oligocene–post Miocene sediments. The Cretaceous and Eocene deposits occupy the troughs of synformal-like folds within the crystalline hill ranges. Gebel Atshan, Gebel Abu Had, and Gebel El Gir are good examples of the pre-rift series outcrops in Quseir and Nile Valley basins, where more than 500 m of Cretaceous and Eocene deposits are exposed from bottom to top. These basins have evolved as a result of structural differentiation and subsidence of the rigid cratonic plate (El-Hawat 1997). Precambrian crystalline basement highs separate these basins and are believed to be the main source for terrigenous sediments during Phanerozoic time. The marine upper Eocene and Oligocene deposits are absent, indicating that the region must have undergone elevation changes during these two epochs (Said 1992). Faulting with a dominant NW trend is the main feature in the region and forms complicated horsts and grabens with outcropping basement rocks covering the major part of this region.

The Paleocene was ushered in by a transgression, which pushed its way across the southern borders of Egypt into North Sudan. The maximum transgression occurred during the Late Paleocene. After the Paleocene, the sea kept retreating toward the North almost continuously except for short intervals (Said 1990). The Lower Paleocene succession in the Nile Valley basin forms a tripartite subdivision arranged in an ascending order by the upper Dakhla Shale (Said 1962), the Tarawan Chalk (Awad and Ghobrial 1965), and the Esna Shale (Zittel 1883) (Fig. 2).

Sampling and methods

Eighteen representative shale samples were collected from the Dakhla Formation from three exposed sections at Gebel Atshan, Gebel Abu Had, and Gebel El Gir in central Egypt (Fig. 2). The petrographic characteristics of six selected mudstone samples were determined through thin section microscopic observations. The clay fractions were subjected to X-ray diffraction analysis to identify their clay mineral composition following the method described by Moore and Reynolds (1997). Three oriented mounts were prepared from each sample: untreated, glycolated, and heated at 600 °C for 1 h. Semiquantitative determination of the identified clay minerals was undertaken based on the method adopted by Hardy and Tucker (1988). X-ray diffractograms were obtained using Philips X-ray diffractometer model PW/1710 with monochromator, Cu radiation (λ=1.542 Å) at 40 KV, 35 mA and scanning speed of 0.02°/s. Also, the samples were scanned by a scanning electronic microscope (SEM, 3.5 nm of resolution) equipped with an energy-dispersive spectrometer (EDS), to determine the chemical composition during SEM observations.

The major oxides and the trace elements were determined in 18 bulk samples using X-ray fluorescence spectrometer (XRF). The correlation coefficient and one-way analysis of variance (ANOVA) have been carried out for the chemical data by using the method of Davis (1986). X-ray fluorescence spectrometry technique, X-ray diffraction (XRD), and SEM-EDS analyses were performed at the laboratories of the National Research Center and Nuclear Materials Authority of Egypt. Analytical precision is better than 5 % for the major oxides and trace elements. Loss on ignition (LOI) was estimated by firing the dried sample at 1000 °C for 2 h. Major element data were recalculated to an anhydrous (LOI-free) basis and adjusted to 100 % before using them in various diagrams. The total iron is expressed as Fe_2O_3.

Results

Petrography

The Dakhla Shales are generally made up of highly foraminiferal argillaceous matrix with minor silt-sized and very fine to fine quartz grains (Fig. 4a, b). The sand-sized grains average 25 % of the rock content. They are generally poorly sorted, subangular to angular, and commonly monocrystalline and exhibit either uniform or undulose extinction (Fig. 4b). Iron oxides, averaging 3 % of the rock content, are commonly present in the form of a very fine material replacing the clay matrix or as dark patches. This indicates that these iron oxides are authigenic and were either precipitated by moving fluids or resulted by the degradation and breakdown of iron-rich minerals and detrital ferromagnesian silicates. Scattered opaque grains are occasionally recorded. In some samples, the argillaceous matrix is color-laminated (Fig. 4b). This lamination resulted from the alteration of iron oxide-rich and organic matter-rich laminae.

Mineralogy

The results of the XRD analysis are illustrated in Fig. 3 and summarized in Table 1. The clay mineral (<2 μm) distribution of the Late Cretaceous–Early Tertiary Dakhla Shales displays a fairly constant composition. Smectite and kaolinite constitute the most abundant clay minerals (mean=36 %). Their values increase from the east

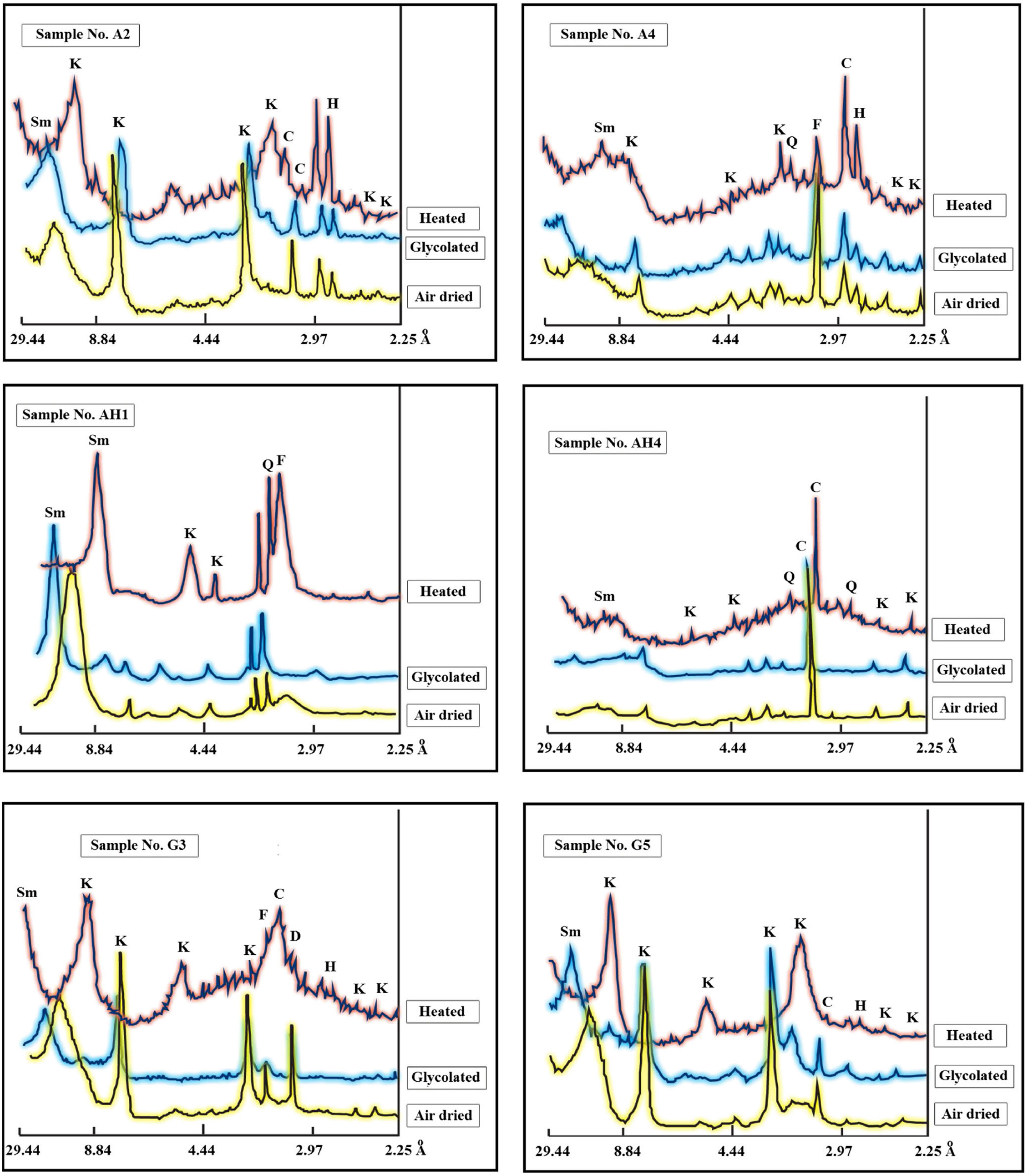

Fig. 3 X-ray diffractograms of six samples of the Dakhla Shale. *Sm* smectite, *K* kaolinite, *C* calcite, *F* feldspar, *Q* quartz, *H* hematite

(Quseir: Gebel Atshan) to the west (Nile Valley, Qena area: Gebel Abu Had and Gebel El Gir). The bulk rock mineralogy indicates the presence of phyllosilicates with abundant quartz and calcite, anhydrite, some dolomite, iron oxides, phosphate, feldspars, and gypsum. Quartz is the most abundant nonclay minerals (average=25 %) followed by carbonates (average=26 %), sulfates (average=8 %), iron oxide (up to 3 %), fluorapatite (up to 2 %), pyrite (up to

Table 1 Semiquantitative mineralogical composition of whole rock and <2 μm fraction

Location	Gebel Atshan						Gebel Abu Had						Gebel El Gir						Average
	A1	A2	A3	A4	A5	A6	AH1	AH2	AH3	AH4	AH5	AH6	G1	G2	G3	G4	G5	G6	
Quartz	27	30	33	50	20	14	19	74	30	28	47	0	14	16	17	7	7	19	25
Feldspar	0	0	0	4	0	0	0	0	0	3	9	0	1	3	0	0	0	0	1
Calcite	54	56	0	0	38	52	68	0	0	8	0	0	0	0	42	0	88	0	23
Dolomite	0	0	0	0	0	0	0	0	0	0	0	0	0	0	3	0	0	51	3
Anhydrite	0	0	0	0	0	0	0	0	0	0	4	84	0	0	0	44	0	0	7
F-apatite	10	0	0	0	0	0	0	0	0	0	0	0	0	0	0	0	0	17	2
Iron oxides	0	0	0	5	0	0	0	0	10	0	0	0	0	39	2	5	0	0	3
Pyrite	0	0	2	0	0	0	1	0	0	0	0	0	0	0	0	0	0	0	0
Gypsum	0	0	1	0	0	0	0	6	0	0	0	0	0	0	3	0	0	0	1
Clay minerals	9	14	64	41	42	34	12	20	60	69	40	16	85	42	33	44	5	13	36
MMI	25.0	31.8	66.0	43.2	67.7	70.8	38.7	21.3	66.7	69.0	41.7	100.0	85.0	68.9	66.0	86.3	41.7	40.6	57
<2 μm clay Sm	15	86	37	31	38	88	55	12	87	91	75	95	31	35	34	52	32	37	52
K	85	14	63	69	62	12	45	88	13	9	25	5	69	65	66	48	68	63	48

Feldspar k-feldspar + plagioclase, *MMI* (Mudrock Maturity Index, *MMI* 100×phyllosilicates/(phyllosilicates + quartz + feldspars; Bhatia 1985), *Sm* smectite, *K* kaolinite

1 %), and K-feldspar and plagioclases (up to 1 %). The mineralogical composition indicates a high mudrock maturity index (MMI=100×phyllosilicates/(phyllosilicates + quartz + feldspars; Bhatia 1985), with an average value of 57 (Table 1).

Clay minerals

Smectite Smectite (Fig. 4c) is the dominant constituent of the clay mineral content of the Dakhla Shales at Quseir and Nile Valley. The average content of smectite in the samples ranges

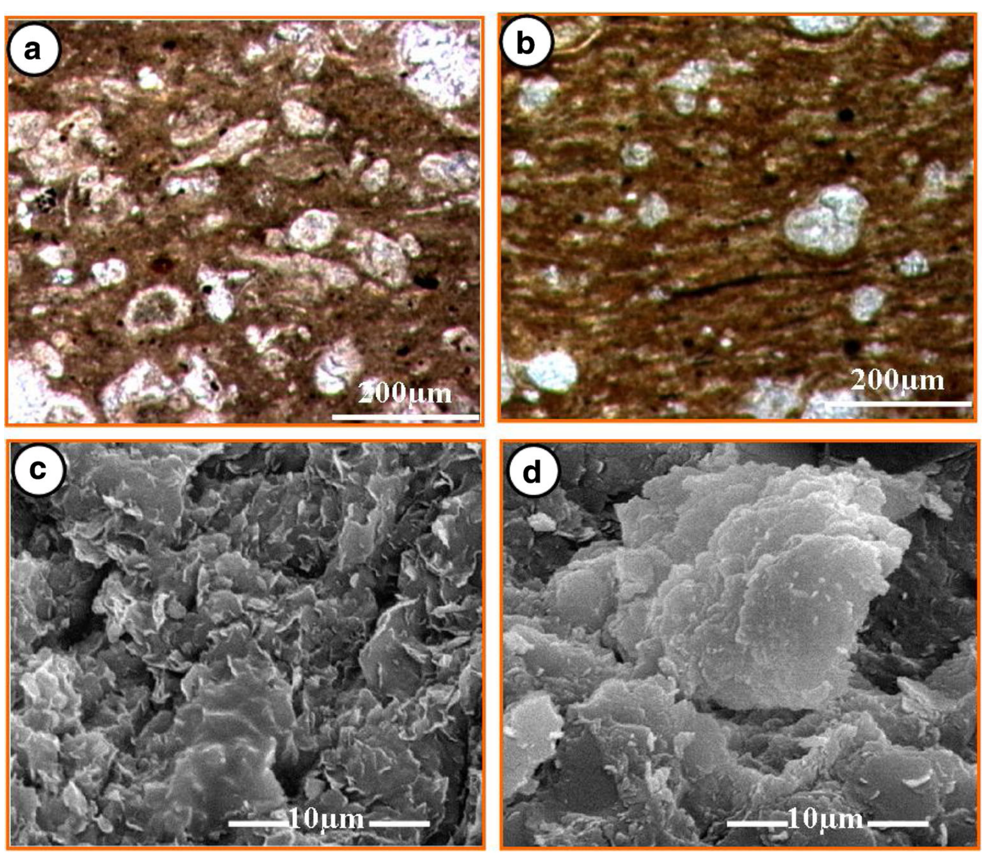

Fig. 4 **a** Photomicrograph showing highly foraminiferal shale (Gebel El Gir); **b** photomicrograph of laminated foraminiferal shale showing fine, monocrystalline quartz grains embedded in an argillaceous matrix stained with iron oxides (Gebel Atshan); **c** SEM photomicrograph shows detrital platelets and coarse detrital kaolinite with irregular edges (Gebel Abu Had); **d** SEM photomicrograph shows smectite particles (Gebel Atshan)

from 12 to 95 % (Table 1). The dominance of smectite in central Egypt is in agreement with the obtained results from Hendriks (1985, 1988), Hendriks et al. (1990), Ismael (1996), and Ahmed (1997). They attributed a continental pedogenetic origin as well as marine neoformation. Terrestrial smectite developed under warm and humid to seasonally humid conditions by the degradation of chlorite and illite or by crystallization from ion-enriched hydrolytic solutions in badly drained alkaline soils (Ahmed 1997).

There are four main genetic hypotheses for the origin of smectite: (1) reworking of soils and enrichment by differential settling, (2) alteration of volcanic material, (3) transformation of detritals, and (4) authigenesis (Chamley 1989; Thiry and Jaquin 1993). The absence of any conceivable volcanic precursor, such as tuff or glass in the studied shales, indicates that smectite is mainly of a detrital origin. Hendriks et al. (1990) suggested a warm/humid climate proven by the smectite rich in diverse fauna and flora in central Egypt. Discrete smectite is commonly forming from the weathering of ultrabasic or very basic rocks which produce magnesium minerals (Surdam and Stanley 1979).

The smectite–kaolinite association in the studied Dakhla Shales does not suggest the formation of kaolinite under the same conditions of smectite formation or the in situ formation of kaolinite by chemical precipitation. Smectite formation is compatible with alkaline reducing conditions, while kaolinite is generally thought to require acid conditions, and it may be unstable in alkaline environments. The occurrence of smectite together with kaolinite indicates the alteration of feldspar in connection with an "arenization" (Millot 1970) of crystalline basement rocks in a warm and semiarid climate. Generally, the clay mineral associations in the studied shales at Nile Valley and Quseir with its smectite dominance suggest a terrestrial provenance (Hendriks et al. 1990) that had not attained intensive weathering, under a warm and semiarid climate. The weathered materials were carried by fluvial action, which finally interfered and admixed with marine environments.

Kaolinite Kaolinite (Fig. 4d) is the dominant clay mineral of Dakhla Shales at Gebel Abu Had and Gebel Atshan. The average content of kaolinite in the shales varies between 5 and 88 % (Table 1). The origin of kaolinite in the studied shales has been previously interpreted as being a product of chemical weathering and leaching of rocks which occur especially in the exposed granite–metamorphic basement areas of central Egypt (Gindy 1983). Kaolinite formation is favored under tropical to subtropical humid climatic conditions (Chamley 1989; Hallam et al. 1991). In addition to a detrital origin, kaolinite may also develop by diagenetic processes due to the circulation of acid solutions (Ghandour et al. 2003). The amount of kaolinite in the shales of Late Cretaceous–Early Tertiary Dakhla Shale in the Nile Valley and Quseir sections is in agreement with the results obtained by Hendriks et al. (1990), Ismael (1996), and Ahmed (1997). This kaolinite represents a continental weathering product at a warm and at least seasonally humid climate, being eroded and transported toward the sea by rivers.

Nonclay minerals

Quartz Quartz was found occurring as an important nonclay mineral in all samples. Quartz contents are recorded with relatively low to moderate abundance. It varies from 7 to 74 %. The relatively higher quartz abundances were obtained from the Dakhla Shale sediments at Gebel Abu Had. A negative relationship between quartz and kaolinite (Table 1) suggests that, in addition to detrital origin, kaolinite may also develop by diagenetic processes due to the circulation of acid solutions (Ghandour et al. 2003).

Carbonates The carbonate minerals detected by XRD are calcite and dolomite. Calcite is recorded with high abundance in the bulk and clay-size mineralogy. It ranges from 0 to 88 % of the bulk rock mineralogy. Generally, the Lower Tertiary sediments at Gebel El Gir contain higher calcite contents than the other locations. On the other hand, dolomite was detected in a number of samples. It reaches up to 51 % in sample G6. The high content of calcite in the Dakhla Shales is consistent with the abundance of calcareous microfossils (Faris et al. 1999) and confirms the biogenic origin of the mineral.

Sulfates Anhydrite is almost absent, being abundant (up to 84 % in AH6) only in a few samples. The relatively higher anhydrite abundances were obtained from the Gebel Abu Had. It was identified in the XRD diffractograms by its characteristic lines at 3.50 and 2.85 Å. Gypsum was identified in a number of samples by its characteristic lines at 7.56, 3.06, and 4.27 Å. It reaches a maximum value of 6 % in sample AH2. The evaporites form from saline-rich fluids–brines. Brines may be generated by the concentration of sea water, by evaporation or freezing, or as residual connate fluids in the subsurface (Selley 1988). Secondary brines can form where meteoric groundwater dissolves previously formed evaporites.

Anhydrite and gypsum in the studied shales were probably precipitated primarily as metal sulfides under reducing conditions when the shales were deposited. After the compaction of shales and oxidation of sulfides to sulfates resulting at least in part of biological activity, the produced sulfates react with the calcic cement generated by weathering of carbonate to form gypsum. These dissolved sulfates will be expelled by solution due to the compaction of clays and concentrate along bedding planes as gypsiferous bands or streaks which can be easily seen in the field.

Iron oxides Iron oxides are almost absent, being abundant (up to 39 % in G2) only in few samples. The relatively higher hematite abundances were obtained from the Gebel El Gir. Iron oxides can be formed either by pedogenic processes or by the precipitation of iron oxides from laterally flowing surface or groundwater (Ollier and Galloway 1990).

Carbonate fluorapatite The phosphate minerals encountered in Quseir and Nile Valley sections are carbonate fluorapatite, which are traditionally called francolite. This mineral is always the sole constituent of phosphorites in unweathered or only slightly weathered sedimentary deposits, whatever their age or location (Prevot et al. 1989). The peak area under the 2.79 Å is taken as the relative abundance of francolite. It reaches up to 17 % in sample G6.

The presence of francolite, calcite, and dolomite in the shales of the Nile Valley and Quseir sections indicates their deposition in a marine environment. The precipitation of phosphorites relates to the upwelling of nutrient-rich water (Selley 1988). Germann et al. (1987) concluded that the origin of the Egyptian phosphorites can be attributed to four distinct genetic phases, namely primary enrichment, secondary concentration, lithification, and weathering. The primary enrichment phase under suboxic to anoxic environment during transgression is producing phosphatic shales. The secondary concentration phase under oxic environment is settling during regression and producing phosphatic sands and shales (Germann et al. 1987). The lithification phase in an oxic/anoxic facies controlled by permeability, chemistry of the host rocks, and pore fluids is producing calcareous, siliceous, clayey, phosphatic phosphorites, and organic-rich clay and siltstone.

Pyrite Pyrite was only detected in the Dakhla Shales of Gebel Atshan and Gebel Abu Had. It reaches up to 2 % in sample A3. It was identified in the diffractograms by its characteristic lines at 2.71 and 2.42 Å. The presence of pyrite spheres and framboids as seen by the SEM indicates the prevalence of a reducing environment during the deposition. The presence of pyrite spheres may be an indicator of shallow water, such as those found on submarine swells or in areas of nutrient upwelling in shelf settings (Schieber and Baird 2001). Pyrite forms in sediments as a consequence of the bacterial reduction of sea water sulfate. Thus, the highly pyritic shales must have formed under euxinic conditions where H_2S exists above or at least at the sediment–water interface. The presence of H_2S in turn will react with Fe^{2+} which was probably delivered into the basin as colloidal material adsorbed on clay minerals to form iron sulfide. By increasing the activity of the hydrogen sulfide in the presence of iron and organic matter, a hydrophobic sulfide gel might have been formed (El-Dahhar 1987).

Feldspar Feldspar is the less frequent nonclay mineral in Dakhla Shales (Table 1). It varies from 0 to 9 %. Its low values may indicate intensive recycling, dissolution, and kaolinitization.

Geochemistry

The major and selected trace element concentrations of 18 samples of Dakhla Shales are presented in Tables 2 and 3. The major and trace elemental concentrations of the shale in this study are compared with published average shales in Table 4. In general, the bulk compositions of the shale in the present study compare quite closely with the published average shale compositions (Gromet et al. 1984; Pettijohn 1975; Turekian and Wedepohl 1961; Vine and Tourtelot 1970).

Silica (SiO_2) is the dominant constituent of the studied shale samples. Its average is 40.35 wt% and closely concurs with the average shales of Pettijohn (1975). SiO_2 is considered to be dominantly terrigenous in origin. The abundance of SiO_2 and Al_2O_3 in shales may be perturbed from parent material by weathering, transport, and depositional processes (Nesbitt et al. 1980). The average content of Al_2O_3, TiO_2, MgO, Na_2O, and K_2O in the studied shales (10.88, 0.63, 1.62, 0.51, and 1.65 %, respectively) is nearly similar to that of Vine and Tourtelot (1970). The low amount of K_2O reflects the diagenetic effects as the element is easily mobile. The high content of CaO (11.3 %) may be related to biochemical origin and shell fragments so that it is used as marine indicator.

On the Fe_2O_3/K_2O versus SiO_2/Al_2O_3 chemical classification diagram (Fig. 5; Herron 1988), the Dakhla Shales mostly plot in the shale field. The average K_2O/Na_2O ratios of the Dakhla Shale vary from 2.32 to 5.19 (average=3.36); the shale of Gebel El Gir has a lower ratio (average 2.32–4.08) compared to the shale of Gebel Atshan and Gebel Abu Had (average 3.5), which is also evidenced from Fig. 6. The ratio is found higher in the Dakhla Shales in comparison to the North American shale composite (NASC) and post-Archean Australian shale (PAAS) (data of NASC and PAAS are from Condie 1993). However, SiO_2/Al_2O_3 ratios among Dakhla Shales show close variations (average 3.5–4.27, Table 2).

Figure 7a, b shows the distribution of major and selected trace element contents of the shales normalized to PAAS (Taylor and McLennan 1985). Compared to PAAS, the Dakhla Shales are highly enriched in SiO_2, Al_2O_3, Fe_2O_3, Sr, Ba, V, Ni, Cr, Zn, Cu, and Rb and highly depleted in TiO_2, Na_2O, Hf, and Cs contents and moderately depleted in MgO, K_2O, U, Th, Cd, Sc, Zr, Pb, and Co contents. The application of ANOVA at 95 % confidence level reveals that there is no statistically significant difference among the Dakhla Shales at the three studied localities (Gebel Atshan, Abu Had, and Gebel El Gir) in SiO_2, Al_2O_3, CaO, MgO, Fe_2O_3, TiO_2, P_2O_5, Na_2O, Sr, Ba, Zr, Cd, U, Th, Cs, Sc, and Co contents ($P>0.05$), indicating a single source rock (Table 5). Depletion of Na_2O in the shales relative to PAAS suggests either a lesser amount of plagioclase detritus in the shales or comparatively intense chemical weathering at the source and during fluvial transportation of the detrital material of the shales. Depletion of TiO_2 and K_2O indicates the

Table 2 Major element concentrations (wt%) of Dakhla Shale

Location	Gebel Atshan						Gebel Abu Had						Gebel El Gir						Average	PAAS
Sample	A1	A2	A3	A4	A5	A6	AH1	AH2	AH3	AH4	AH5	AH6	G1	G2	G3	G4	G5	G6		
SiO_2	37.73	35.39	46.05	47.75	40.32	36.45	29.08	29.89	46.78	49.63	46.85	42.19	45.54	47.50	45.02	48.11	29.34	22.70	40.35	62.4
Al_2O_3	8.83	8.79	13.07	11.81	11.43	10.16	8.30	8.55	13.13	13.24	12.24	10.99	11.57	12.93	12.86	13.34	8.33	6.24	10.88	18.78
CaO	17.03	21.53	0.83	1.52	16.24	12.33	20.15	33.82	0.08	0.03	0.79	18.40	0.10	0.19	9.29	0.36	28.62	23.40	11.37	1.29
MgO	1.74	1.41	2.14	1.74	2.41	2.01	0.62	0.71	1.40	1.62	1.49	3.16	0.93	1.30	2.80	1.26	0.90	1.59	1.62	2.19
Fe_2O_3*	4.88	3.92	4.77	4.88	6.07	5.87	0.14	3.00	15.25	4.35	6.01	5.22	8.75	24.91	6.08	4.70	3.95	2.14	6.38	7.18
TiO_2	0.44	0.46	0.76	0.69	0.58	0.44	0.23	0.40	0.81	0.99	1.00	0.44	0.91	0.81	0.79	0.96	0.41	0.17	0.63	0.99
P_2O_5	3.32	2.60	0.13	0.51	4.89	5.81	17.75	0.42	0.14	0.06	0.34	0.11	0.09	0.12	0.26	0.05	0.21	6.21	2.39	0.16
Na_2O	0.66	0.69	0.36	0.44	0.76	0.55	0.37	0.38	0.51	0.35	0.53	0.37	0.54	0.66	0.70	0.36	0.61	0.36	0.51	1.19
K_2O	2.64	1.64	1.87	1.81	1.92	1.83	1.05	1.46	1.75	1.59	2.02	1.30	1.59	1.53	1.65	1.47	1.46	1.05	1.65	3.68
SO_3	0.13	0.13	2.42	0.05	0.21	0.23	0.66	0.28	1.03	0.57	0.12	0.57	0.27	0.66	0.14	0.50	0.13	0.94	0.50	–
LOI	22.28	23.30	27.26	28.40	15.85	24.60	20.96	20.70	19.03	27.50	28.60	16.80	29.70	9.36	20.33	28.35	25.50	35.10	23.53	–
Total	99.68	99.86	99.66	99.60	100.68	100.28	99.31	99.61	99.91	99.93	99.99	99.55	99.99	99.97	99.92	99.46	99.46	99.90	99.82	–
Al_2O3/TiO_2	20.07	19.11	17.20	17.12	19.71	23.09	36.09	21.38	16.21	13.37	12.24	24.98	12.71	15.96	16.28	13.90	20.32	36.71	19.80	–
SiO_2/Al_2O_3	4.27	4.03	3.52	4.04	3.53	3.59	3.50	3.50	3.56	3.75	3.83	3.84	3.94	3.67	3.50	3.61	3.52	3.64	3.71	–
K_2O/Na_2O	4.00	2.38	5.19	4.11	2.53	3.33	2.84	3.84	3.43	4.54	3.81	3.51	2.94	2.32	2.36	4.08	2.39	2.92	3.36	–
K_2O/Al_2O_3	0.30	0.19	0.14	0.15	0.17	0.18	0.13	0.17	0.13	0.12	0.17	0.12	0.14	0.12	0.13	0.11	0.18	0.17	0.16	–
CIA	71.01	76.41	85.34	83.84	79.38	79.62	82.34	77.77	85.31	87.22	82.68	84.61	84.44	85.50	83.64	87.90	76.34	77.34	81.70	–
PIA	86.52	86.94	96.76	95.54	90.06	91.54	90.85	87.81	95.70	97.08	94.95	93.28	94.85	94.50	92.83	97.01	85.97	86.97	92.17	–
CIW	90.16	89.11	97.21	96.20	91.59	92.95	91.92	89.68	96.25	97.42	95.74	94.02	95.53	95.12	93.69	97.33	88.14	88.92	93.39	–
CIW`	93.05	92.72	97.32	96.41	93.77	94.86	95.73	95.74	96.26	97.42	95.85	96.74	95.54	95.14	94.84	97.37	93.18	94.55	95.36	–
ICV	3.05	3.32	0.76	0.88	2.40	2.22	2.69	4.60	1.45	0.60	0.89	2.59	1.03	2.21	1.60	0.61	4.27	4.57	2.21	–

*Fe_2O_3** total Fe expressed as Fe_2O_3, *CIA* $[Al_2O_3/(Al_2O_3 + CaO^* + Na_2O + K_2O)] \times 100$ (Nesbitt and Young 1982), *PIA* $[(Al_2O_3 - K_2O)/(Al_2O_3 + CaO^* + Na_2O + K_2O)] \times 100$ (Fedo et al. 1995), *CIW* $[Al_2O_3/(Al_2O_3 + CaO^* + Na_2O)] \times 100$ (Harnois 1988), *CIW'* $((Al_2O_3/(Al_2O_3 + Na_2O)) \times 100$ (Cullers 2000). *CaO** CaO in silicate phase (to calculate CaO*, the assumption proposed by McLennan et al. (1993) was followed), *ICV* = $(Fe_2O_3 + K_2O + Na_2O + CaO + MgO + MnO + TiO_2)/Al_2O_3$ (Cox et al. 1995)

presence of relatively lesser quantities of phyllosilicate minerals in the shales (McCann 1991; Condie et al. 1992). A low content of TiO_2 also suggests evolved (felsic) source rocks.

Major element compositions of the analyzed samples are mainly controlled by clay minerals rather than the nonclay silicate phases. This trend can be illustrated from the values of the index of compositional variation (ICV; Cox et al. 1995) where ICV = $(Fe_2O_3 + K_2O + Na_2O + CaO + MgO + MnO)/Al_2O_3$. ICV values of the shales of the present study are low and vary from 0.6 to 4.57 (average=2.21). Values of ICV<1 are typical of minerals like kaolinite, illite, and muscovite and higher values (>1) are characteristic of rock-forming minerals such as plagioclase, K-feldspar, amphiboles, and pyroxenes. Hence, the shales of the present study are enriched in rock-forming minerals in comparison with clays. Values of K_2O/Al_2O_3 ratio of clays are less than 0.3 and those of feldspars range from 0.3 to 0.9 (Cox et al. 1995). The values of K_2O/Al_2O_3 ratio of the shales of the present study vary narrowly from 0.11 to 0.3 (average=0.16). These values also indicate the predominance of clay minerals over K-bearing minerals such as K-feldspars and micas (Cox et al. 1995; Moosavirad et al. 2011).

The ratios of the abundance of major oxides and correlation coefficient data of major and trace elements of the shales (Tables 2, 3, and 6) reveal other interesting features. Values of Al_2O_3/TiO_2 ratio are high (average=19.8) and indicate derivation of the detrital material from a continental source (Fyffe and Pickerill 1993). SiO_2 exhibits a strong negative correlation with CaO (r=−0.89) and P_2O_5 (r=−0.57), indicating a decrease of calcite and phosphate with increasing contents of quartz. SiO_2 shows positive correlations with Al_2O_3 (r=0.96), TiO_2 (r=0.91), and Fe_2O_3 (r=0.48). Al_2O_3 exhibits covariance with TiO_2 (r=0.90) and Fe_2O_3 (r=0.49). These linear relationships suggest detrital sorting trends. SiO_2 shows a negative correlation with several major elements (Table 6) indicating quartz dilution (Kampunzu et al. 2005; Deru et al. 2007). The positive correlation of TiO_2 with Al_2O_3 and the negative correlations of TiO_2 with several major elements (CaO, MgO, and P_2O_5) suggest that TiO_2 occurs as an essential chemical constituent of clays (kaolinite) rather than of mafic minerals. Al_2O_3 exhibits a positive correlation with K_2O (r=0.27) and a strong positive correlation with SiO_2 (r=0.96). These linear trends point to the presence of kaolinite and a few K-feldspar (Armstrong-Altrin et al. 2015). The values of K_2O/Na_2O ratios (average=3.36) indicate the presence

Table 3 Trace element concentrations in parts per million for shales of the Upper Cretaceous–Lower Tertiary Dakhla Formation, central Egypt

Elements	Gebel Atshan							Gebel Abu Had							Gebel El Gir						
	A1	A2	A3	A4	A5	A6	Average	AH1	AH2	AH3	AH4	AH5	AH6	Average	G1	G2	G3	G4	G5	G6	Average
Sr	486.0	513.0	76.0	128.0	949.0	470.0	437.0	951.0	1030.0	113.0	109.0	156.0	400.0	459.8	54.0	40.0	299.0	263.0	784.0	301.0	290.2
Ba	79.0	93.0	92.0	110.0	98.0	72.0	90.7	110.0	87.0	60.0	69.0	140.0	73.0	89.8	72.0	73.0	74.0	97.0	62.0	34.0	68.7
V	3151.0	2679.0	110.0	160.0	1455.0	1835.0	1565.0	20.0	110.0	180.0	190.0	250.0	140.0	148.3	218.0	202.0	197.0	170.0	140.0	45.0	162.0
Ni	186.0	153.0	41.0	30.0	177.0	126.0	118.8	12.0	60.0	46.0	33.0	46.0	43.0	40.0	64.0	87.0	52.0	34.0	45.0	11.0	48.8
Co	9.0	9.0	20.0	9.0	12.0	8.0	11.2	10.0	3.0	25.0	9.0	12.0	13.0	12.0	18.0	25.0	9.0	8.0	9.0	8.0	12.8
Cr	631.0	414.0	81.0	123.0	540.0	379.0	361.3	35.0	240.0	108.0	163.0	265.0	153.0	160.7	200.0	192.0	224.0	156.0	222.0	28.0	170.3
Zn	1600.0	1130.0	69.0	135.0	1040.0	1250.0	870.7	40.0	61.0	116.0	61.0	90.0	110.0	79.7	195.0	138.0	96.0	68.0	54.0	37.0	98.0
Cu	243.0	178.0	27.0	25.0	154.0	156.0	130.5	10.0	31.0	21.0	29.0	25.0	16.0	22.0	21.0	9.0	25.0	22.0	19.0	9.0	17.5
Zr	93.0	95.0	138.0	146.0	105.0	104.0	113.5	40.0	55.0	91.0	112.0	173.0	55.0	87.7	93.0	87.0	97.0	109.0	52.0	38.0	79.3
Cd	47.0	73.0	1.1	1.3	40.0	15.0	29.6	3.0	7.0	4.0	0.7	4.0	4.0	3.8	3.0	382.0	3.0	3.0	4.0	9.0	67.3
U	41.0	34.0	0.8	9.0	44.0	52.0	30.1	24.0	11.0	3.0	4.0	3.0	5.0	8.3	4.0	380.0	4.0	4.0	3.0	0.6	65.9
Th	9.0	8.0	10.0	7.0	8.0	9.0	8.5	1.0	10.0	9.0	8.0	9.0	9.0	7.7	8.0	9.0	9.0	8.0	9.0	27.0	11.7
Cs	8.0	7.0	6.0	0.6	0.8	8.0	5.1	1.0	1.0	6.0	7.0	0.6	0.7	2.7	0.6	0.5	7.0	0.7	7.0	0.5	2.7
Pb	20.0	29.0	13.0	10.0	30.0	33.0	22.5	10.0	12.0	16.0	13.0	14.0	15.0	13.3	13.0	14.0	13.0	16.0	14.0	15.0	14.2
Sc	9.0	12.0	7.0	7.0	5.0	7.0	7.8	5.2	6.4	5.0	8.3	11.7	12.8	8.2	8.2	10.5	9.8	7.5	7.6	6.6	8.4
Hf	1.2	1.3	0.8	1.1	1.1	1.3	1.1	0.70	0.80	0.60	1.12	1.13	1.56	1.0	1.54	2.01	1.78	1.78	1.47	1.15	1.6
Rb	31.0	30.0	28.0	32.0	40.0	32.0	32.2	10.0	19.0	24.0	26.0	41.0	16.0	22.7	27.0	27.0	25.0	19.0	19.0	10.0	21.2
Ni/Co	20.7	17.0	2.1	3.3	14.8	15.8	12.3	1.2	20.0	1.8	3.7	3.8	3.3	5.6	3.6	3.5	5.8	4.3	5.0	1.4	3.9
Cu/Zn	0.2	0.2	0.4	0.2	0.1	0.1	0.2	0.3	0.5	0.2	0.5	0.3	0.1	0.3	0.1	0.1	0.3	0.3	0.4	0.2	0.2
Th/Sc	1.0	0.7	1.4	1.0	1.6	1.3	1.2	0.2	1.6	1.8	1.0	0.8	0.7	1.0	1.0	0.9	0.9	1.1	1.2	4.1	1.5
Zr/Sc	10.3	7.9	19.7	20.9	21.0	14.9	15.8	7.7	8.6	18.2	13.5	14.8	4.3	11.2	11.3	8.3	9.9	14.5	6.8	5.8	9.4

Table 4 Comparison of the chemical composition of the studied shales with published averages

	Present study	1	2	3	4
SiO_2%	40.35	64.82	58.10	58.50	n.a.
Al_2O_3%	10.88	17.05	15.40	15.00	13.22
TiO_2%	0.63	0.80	n.a.	0.77	0.33
Fe_2O_3%	6.38	5.70	4.02	4.72	2.86
MgO%	1.62	2.83	2.44	2.50	1.77
CaO%	11.37	3.51	3.11	3.10	2.10
Na_2O%	0.51	1.13	1.30	1.30	0.94
K_2O%	1.65	3.97	3.24	3.10	2.41
P_2O_5%	2.39	0.15	n.a.	0.16	n.a.
Sr (ppm)	396	142	n.a.	300	200
Ba (ppm)	83	636	n.a.	580	300
V (ppm)	625	130	n.a.	130	150
Ni (ppm)	69	58	n.a.	68	50
Cr (ppm)	231	125	n.a.	90	100
Zn (ppm)	349	n.a.	n.a.	95	300
Cu (ppm)	57	n.a.	n.a.	45	70
Zr (ppm)	94	200	n.a.	160	n.a.

1 = NASC (Gromet et al. 1984); 2 = average shale (Pettijohn 1975); 3 = average shales (Turekian and Wedepohl 1961); 4 = average black shales (Vine and Tourtelot 1970)

n.a. no average

of K-bearing minerals such as K-feldspar, muscovite, and biotite. Although Na_2O exhibits very weak positive correlations with SiO_2, Al_2O_3, CaO, MgO, and TiO_2, it shows positive correlations with Fe_2O_3 (r=0.36) and a negative correlation with P_2O_5 (r=−0.10), suggesting the presence of smectite (Nagarajan et al. 2007). CaO exhibits a strong negative correlation with SiO_2 (r=−0.89), indicating that the dominance of calcite over other minerals in the bulk fraction is consistent with the high abundance of calcareous fossils (Faris et al. 1999).

The Late Cretaceous/Early Tertiary Dakhla Shales are lower in large ion lithophile trace elements (Rb, Cs, and Ba) and transition trace elements (Co, Ni, Sc, and Cu), in comparison to PAAS (Taylor and McLennan 1985) (Fig. 7b). As correlations are concerned (Table 6), certain trace elements like Zr, Co, Rb, Ba, and Hf are positively correlated with Al_2O_3 (r= 0.66, 0.53, 0.44, 0.26, and 0.23, respectively; n=18), indicating that these elements are likely fixed in K-feldspars and clays. On the other hand, the correlation of Al_2O_3 versus Sc, Cd, U, Ni, Cr, Pb, V, Zn, Cu, and Sr is very low or negative (r=0.12, 0.15, 0.17, −0.12, −0.13, −0.15, −0.17, −0.26, −0.27, and −0.62, respectively; n=18), indicating that they are not likely bound in the clay minerals (Armstrong-Altrin 2009). Also, Cu and Cr positively correlated with CaO, MgO, Na_2O, and K_2O, suggesting their occurrence in mafic mineral components of the shales (Table 6).

Gebel Abu Had and Gebel Atshan reported a significant difference (P<0.05) in K_2O, V, Ni, Cr, Cu, Pb, and Rb, compared to those recorded in Gebel El Gir (Qena area), suggesting their presence as absorbed ions in clay minerals. However, the application of ANOVA at 95 % confidence level reveals a significant difference among the three studied localities in Zn and Hf contents (Table 5) and indicates that these elements are hosted by clay minerals.

Discussion

Weathering and sediment recycling

Most of the labile material (about 75 %) of the upper crust is composed of feldspars and volcanic glass, and chemical weathering of these materials ultimately results in the

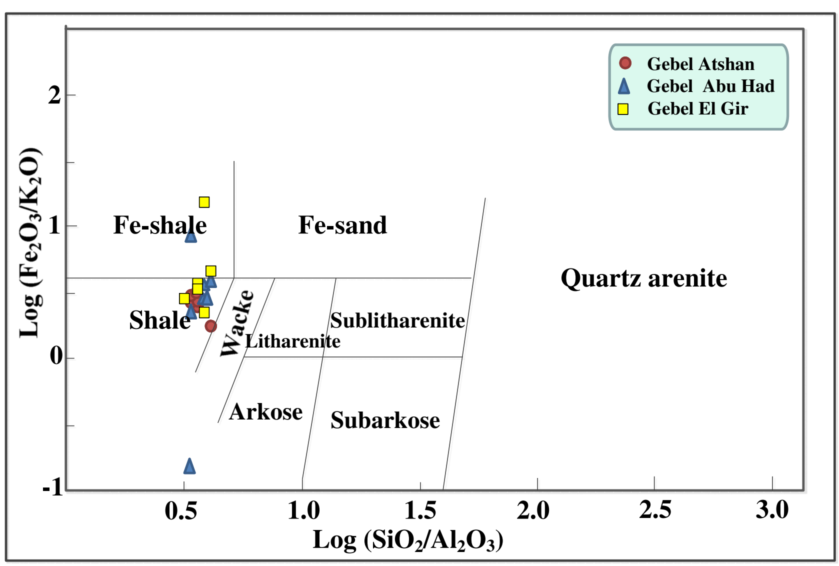

Fig. 5 Geochemical classification diagram using log (SiO_2/Al_2O_3)–log (Fe_2O_3/K_2O) (after Herron 1988)

Fig. 6 SiO_2/Al_2O_3 versus K_2O/Na_2O bivariate plot

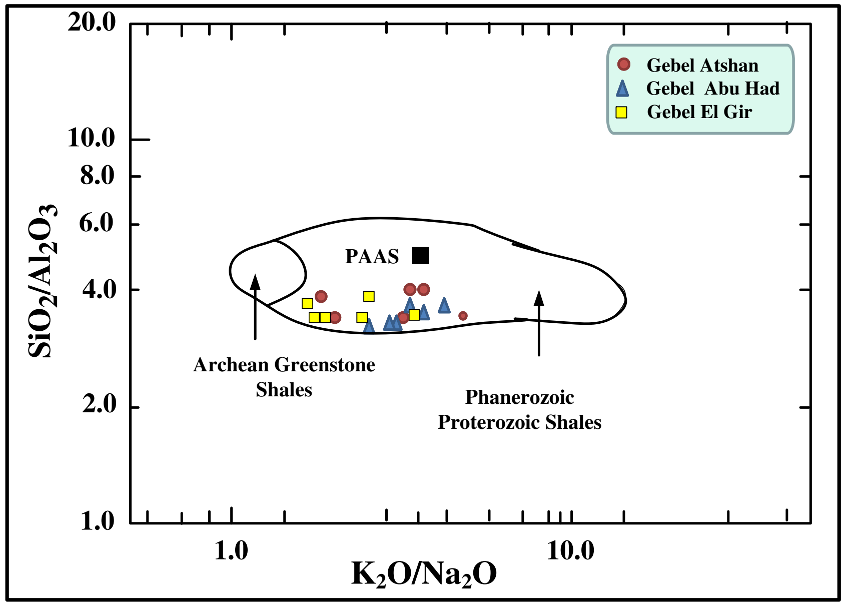

formation of clay minerals (e.g., Nesbitt and Young 1984, 1989). The intensity and duration of weathering in clastic sediments can also be evaluated by examining the relationship between alkali and alkaline earth elements (Nesbitt and Young 1982). The degree of source weathering is quantified variously. A few indices of weathering have been proposed based on abundances of mobile and immobile element oxides (Na_2O, CaO, K_2O, and Al_2O_3). Among the known indices of weathering/alteration, the chemical index of alteration (CIA, Nesbitt and Young 1982) is well established as a method of quantifying the degree of source weathering. Source weathering and elemental redistribution during diagenesis can also be assessed using plagioclase index of alteration (PIA, Fedo et al. 1995) and chemical index of weathering

Fig. 7 Distribution of PAAS normalized abundance of Dakhla Shale: **a** major and **b** trace elements

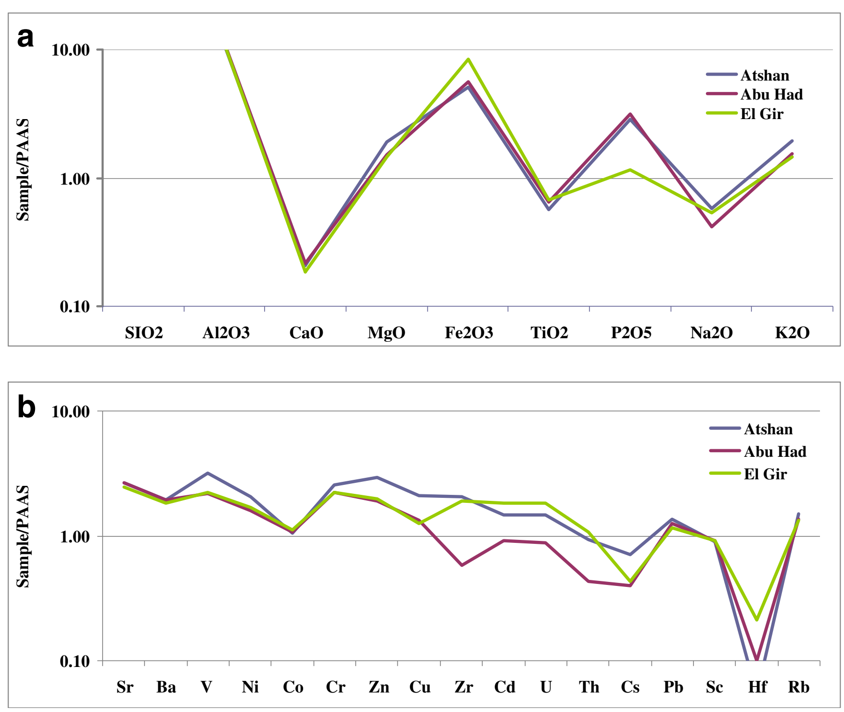

Table 5 Results of successive application of ANOVA at 95 % confidence level to element concentration data for Dakhla Shale

	Location	No.	Mean±std error	Sig. between groups	
SiO_2	1. G. Atshan	6	40.615±2.109[a]	0.975	N sig
	2. G. Abu Had	6	40.736±3.690[a]	0.858	N sig
	3. G. El Gir	6	39.701±4.435[a]	0.896	N sig
Al_2O_3	1. G. Atshan	6	10.681±0.703[a]	0.958	N sig
	2. G. Abu Had	6	11.075±2.901[a]	0.886	N sig
	3. G. El Gir	6	10.878±1.193[a]	0.804	N sig
CaO	1. G. Atshan	6	11.580±3.501[a]	0.956	N sig
	2. G. Abu Had	6	12.376±5.688[a]	0.859	N sig
	3. G. El Gir	6	10.326±5.207[a]	0.815	N sig
MgO	1. G. Atshan	6	1.923±0.359[a]	0.489	N sig
	2. G. Abu Had	6	1.830±0.890[a]	0.264	N sig
	3. G. El Gir	6	1.463±0.703[a]	0.696	N sig
Fe_2O_3	1. G. Atshan	6	5.065±0.323[a]	0.564	N sig
	2. G. Abu Had	6	5.662±2.094[a]	0.323	N sig
	3. G. El Gir	6	8.422±3.419[a]	0.709	N sig
TiO_2	1. G. Atshan	6	0.562±0.056[a]	0.765	N sig
	2. G. Abu Had	6	0.645±0.135[a]	0.487	N sig
	3. G. El Gir	6	0.675±0.128[a]	0.849	N sig
P_2O_5	1. G. Atshan	6	2.877±0.932[a]	0.722	N sig
	2. G. Abu Had	6	3.137±2.923[a]	0.524	N sig
	3. G. El Gir	6	1.157±1.011[a]	0.631	N sig
Na_2O	1. G. Atshan	6	0.577±0.063[a]	0.129	N sig
	2. G. Abu Had	6	0.418±0.032[a]	0.622	N sig
	3. G. El Gir	6	0.538±0.060[a]	0.052	N sig
K_2O	1. G. Atshan	6	1.952±0.143[a]	0.029	Sig
	2. G. Abu Had	6	1.528±0.139[b]	0.014	Sig
	3. G. El Gir	6	1.458±0.086[b]	0.269	N sig
Sr	1. G. Atshan	6	437.00±128.73[a]	0.657	N sig
	2. G. Abu Had	6	459.83±173.74[a]	0.470	N sig
	3. G. El Gir	6	290.17±110.02[a]	0.583	N sig
Ba	1. G. Atshan	6	90.666±5.535[a]	0.191	N sig
	2. G. Abu Had	6	89.833±12.300[a]	0.110	N sig
	3. G. El Gir	6	68.666±8.381[a]	0.380	N sig
V	1. G. Atshan	6	1565.0±514.21[a]	0.025	Sig
	2. G. Abu Had	6	431.67±293.32[b]	0.011	Sig
	3. G. El Gir	6	162.0±25.947[b]	0.319	N sig
Ni	1. G. Atshan	6	118.83±27.72[a]	0.012	Sig
	2. G. Abu Had	6	40.00±6.618[b]	0.013	Sig
	3. G. El Gir	6	48.833±10.587[b]	0.060	N sig
Co	1. G. Atshan	6	11.167±1.851[a]	0.904	N sig
	2. G. Abu Had	6	12.00±2.966[a]	0.659	N sig
	3. G. El Gir	6	12.833±2.891[a]	1.000	N sig
Cr	1. G. Atshan	6	361.33±90.021[a]	0.047	Sig
	2. G. Abu Had	6	160.67±34.549[b]	0.035	Sig
	3. G. El Gir	6	170.33±30.201[b]	0.162	N sig
Zn	1. G. Atshan	6	870.67±255.318[a]	0.002	Sig
	2. G. Abu Had	6	79.667±12.406[b]	0.002	Sig
	3. G. El Gir	6	98.00±24.200[b]	0.042	Sig
Cu	1. G. Atshan	6	130.50±35.570[a]	0.002	Sig
	2. G. Abu Had	6	22.00±3.265[b]	0.002	Sig
	3. G. El Gir	6	17.50±2.801[b]	0.058	N sig

Table 5 (continued)

	Location	No.	Mean±std error	Sig. between groups	
Zr	1. G. Atshan	6	113.50±9.276[a]	0.250	N sig
	2. G. Abu Had	6	87.667±20.241[a]	0.115	N sig
	3. G. El Gir	6	79.333±11.392[a]	0.628	N sig
Cd	1. G. Atshan	6	29.567±11.720[b]	0.490	N sig
	2. G. Abu Had	6	3.783±0.828[a]	0.481	N sig
	3. G. El Gir	6	67.333±62.940[a]	0.339	N sig
U	1. G. Atshan	6	30.133±8.387[a]	0.546	N sig
	2. G. Abu Had	6	8.333±3.363[a]	0.500	N sig
	3. G. El Gir	6	65.933±62.851[a]	0.390	N sig
Th	1. G. Atshan	6	8.500±0.428[a]	0.339	N sig
	2. G. Abu Had	6	7.667±1.358[a]	0.270	N sig
	3. G. El Gir	6	11.667±3.073[a]	0.329	N sig
Cs	1. G. Atshan	6	5.067±1.413[a]	0.376	N sig
	2. G. Abu Had	6	2.717±1.205[a]	0.230	N sig
	3. G. El Gir	6	2.717±1.354[a]	0.481	N sig
Pb	1. G. Atshan	6	22.50±3.922[a]	0.026	Sig
	2. G. Abu Had	6	13.333±0.881[b]	0.024	Sig
	3. G. El Gir	6	14.167±0.477[b]	0.101	N sig
Sc	1. G. Atshan	6	7.833±0.980[a]	0.931	N sig
	2. G. Abu Had	6	8.233±1.364[a]	0.720	N sig
	3. G. El Gir	6	8.367±0.608[a]	0.917	N sig
Hf	1. G. Atshan	6	1.133±0.076[b]	0.004	Sig
	2. G. Abu Had	6	0.985±0.145[b]	0.011	Sig
	3. G. El Gir	6	1.622±0.122[a]	0.016	Sig
Rb	1. G. Atshan	6	32.167±1.681[a]	0.050	Sig
	2. G. Abu Had	6	22.667±4.348[b]	0.024	Sig
	3. G. El Gir	6	21.167±2.688[b]	0.310	N sig

Means with different superscripts in each group (locality) differed significantly ($P<0.05$)

Sig significant, *N sig* non significant

(CIW, Harnois 1988). For quantifying source weathering of carbonate-bearing siliciclastic rocks, a modified version of CIW′ (Cullers 2000) has also been used (e.g., Jafarzadeh and Hosseini-Barzi 2008).

Following the procedure of McLennan (1993), the CIA, PIA, and CIW values of the shales have been determined and the results along with CIW′ values are provided in Table 2. According to CIA values, the degree of source weathering varies from 71.01 to 87.9 % (average=81.7 %). The average CIA is within the range of the PAAS (70–75; Taylor and McLennan 1985). These values indicate a moderate to intense chemical weathering in the source area. The Dakhla Shales have a moderate range in CIA values (71–87; Table 2), indicating mature sediments, which is consistent with the SiO_2/Al_2O_3 ratios (Fig. 5). PIA values indicate the intensity of alteration of source material varying from 85.97 to 97.08 % (average=92.17 %). CIW values suggest the degree of source weathering in the range from 88.14 to 97.42 % (average=93.39 %). CIW′ values vary from 92.72 to 97.42 % (average 95.36 %). Average PIA and CIW values (92 and 93 %, respectively) also indicate a high degree of weathering.

The CIA values are also plotted in Al_2O_3–(CaO^* + Na_2O)–K_2O (A–CN–K) triangular diagram (molecular proportion; Fedo et al. 1996; Fig. 8) which identifies the differentiation of compositional changes associated with chemical weathering and/or source rock composition (Deepthi et al. 2012; Ghosh et al. 2012). The Dakhla Shale plot defines a narrow linear trend and the trend line runs parallel to the A–CN line (Fig. 8) and defines a nonsteady-state weathering trend toward "A." This is primarily due to removal rates of Na and Ca from plagioclase being generally greater than the removal rates of K from microcline (Nesbitt and Young 1984). This nonsteady-state weathering indicates balanced rates of chemical weathering and erosion, which produces

Table 6 Values of Pearson's coefficient of correlation of major and trace elements in shales

	SiO_2	Al_2O_3	CaO	MgO	Fe_2O_3	TiO_2	P_2O_5	Na_2O	K_2O	Sr	Ba	V	Ni	Co	Cr	Zn	Cu	Zr	Cd	U	Th	Cs	Pb	Sc	Hf	Rb
SiO_2	1																									
Al_2O_3	0.959**	1																								
CaO	−0.892**	−0.861**	1																							
MgO	0.075	0.115	−0.009	1																						
Fe_2O_3	0.478*	0.495*	−0.486*	−0.209	1																					
TiO_2	0.911**	0.903**	−0.861**	−0.201	0.428	1																				
P_2O_5	−0.573*	−0.531*	0.358	0.366	−0.369	−0.617**	1																			
Na_2O	0.051	0.020	0.066	0.008	0.359	0.036	−0.103	1																		
K_2O	0.391	0.272	−0.281	−0.039	0.127	0.310	−0.312	0.487*	1																	
Sr	−0.700**	−0.622**	0.839**	0.088	−0.475*	−0.680**	0.524*	0.142	−0.168	1																
Ba	0.311	0.261	−0.226	0.105	−0.186	0.292	0.124	0.024	0.295	0.116	1															
V	−0.038	−0.171	0.127	0.026	−0.135	−0.119	0.072	0.441	0.593**	0.133	−0.013	1														
Ni	−0.040	−0.125	0.186	0.030	0.125	−0.144	0.008	0.746**	0.658**	0.282	0.062	0.805**	1													
Co	0.496*	0.527*	−0.589*	−0.015	0.796**	0.418	−0.228	0.144	0.091	−0.554*	−0.126	−0.256	−0.047	1												
Cr	−0.035	−0.133	0.224	0.001	−0.018	−0.089	−0.054	0.724**	0.728**	0.334	0.153	0.799**	0.950**	−0.231	1											
Zn	−0.149	−0.258	0.212	0.114	−0.075	−0.279	0.177	0.588*	0.641**	0.265	0.030	0.880**	0.931**	−0.193	0.893**	1										
Cu	−0.155	−0.266	0.246	0.088	−0.147	−0.268	0.146	0.568*	0.670**	0.297	0.068	0.908**	0.927**	−0.251	0.909**	0.988**	1									
Zr	0.736**	0.666**	−0.717**	−0.026	0.129	0.726**	−0.421	0.127	0.630**	−0.534*	0.607**	0.143	0.121	0.177	0.181	0.100	0.118	1								
Cd	0.162	0.152	−0.169	−0.161	0.801**	0.102	−0.098	0.392	0.012	−0.194	−0.089	0.052	0.269	0.487*	0.113	0.082	0.028	−0.046	1							
U	0.167	0.172	−0.190	−0.117	0.804**	0.095	−0.041	0.355	0.002	−0.173	−0.078	0.014	0.240	0.481*	0.090	0.071	0.003	−0.047	0.987**	1						
Th	−0.393	−0.381	0.211	−0.164	−0.053	−0.279	−0.140	−0.161	−0.207	−0.191	−0.596**	−0.114	−0.149	−0.094	−0.172	−0.096	−0.101	−0.239	−0.020	−0.063	1					
Cs	−0.005	0.003	0.058	0.048	−0.090	−0.026	−0.116	0.309	0.428	−0.034	−0.295	0.586*	0.345	−0.062−	0.353	0.448	0.480*	0.077	−0.157	−0.171	−0.100	1				
Pb	−0.147	−0.154	0.190	0.132	−0.019	−0.219	0.127	0.538*	0.343	0.266	−0.044	0.684**	0.798**	−0.133−	0.714**	0.831**	0.793**	0.082	0.065	0.062	0.019	0.356	1			
Sc	0.258	0.125	−0.085	0.126	0.160	0.203	−0.397	0.212	0.110	−0.324	0.145	0.187	0.128	0.024	0.174	0.068	0.074	0.185	0.294	0.222	−0.026	0.040	0.020	1		
Hf	0.262	0.229	−0.180	−0.003	0.371	0.265	−0.372	0.356	−0.076	−0.286	−0.178	−0.023	0.106	0.042	0.123	0.000	−0.052	−0.013	0.481*	0.466	0.044	−0.087	0.057	0.573*	1	
Rb	0.521*	0.437	−0.417	−0.035	0.234	0.489*	−0.341	0.574*	0.790**	−0.212	0.488*	0.442	0.595**	0.157	0.630**	0.495*	0.495*	0.813**	0.128	0.122	−0.259	0.174	0.460	0.186	0.026	1

Asterisks denote significant values which show positive (direct) or negative (inverse) relationship between different variables

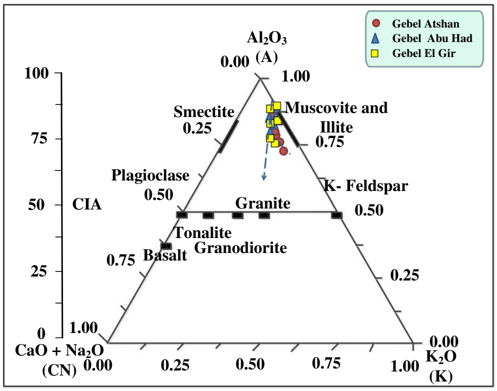

Fig. 8 A–CN–K ternary diagram of molecular proportions of Al_2O_3–(CaO* + Na_2O)–K_2O (after Nesbitt and Young 1982)

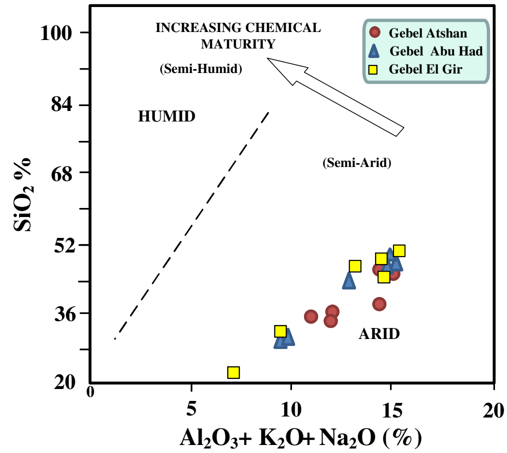

Fig. 10 SiO_2 versus (Al_2O_3 + K_2O + Na_2O) bivariate plot (after Suttner and Dutta 1986)

compositionally similar sediments over a long period (Nesbitt et al. 1997; Selvaraj and Chen 2006).

McLennan et al. (1993) observed that the Th/Sc ratio is a sensitive index of the bulk composition of the provenance, and the Zr/Sc ratio is a useful index of zircon enrichment. Thus, the Th/Sc versus Zr/Sc bivariate plot can be used to discriminate the compositional variation, the degree of sediment recycling, and heavy mineral sorting (Long et al. 2012; Yan et al. 2012). On the Th/Sc–Zr/Sc diagram (Fig. 9), the shales display two compositional trends with most samples gathered near average UCC composition, parallel to trend 2 and few samples plotted along trend 1, which is indicative of a high influence of sediment recycling and mineral sorting.

Suttner and Dutta (1986) proposed a binary SiO_2% versus (Al_2O_3 + K_2O + Na_2O)% diagram to constrain the climatic condition during sedimentation of siliciclastic rocks. On this diagram, the shales plot in the field of arid to semiarid climate (Fig. 10), indicating that the shales of the present study were deposited under arid to semiarid conditions.

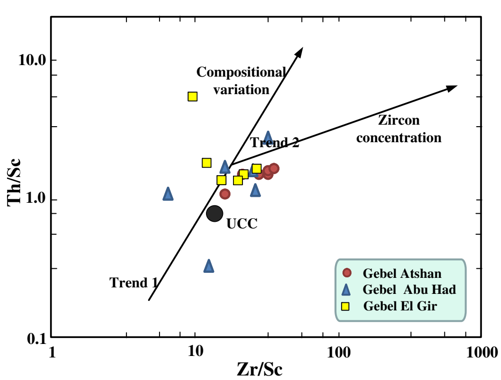

Fig. 9 Th/Sc versus Zr/Sc bivariate plot of Dakhla Shale (McLennan et al. 1993). The addition of zircon due to sediment sorting and recycling is observed in trend 2

Provenance

The geochemistry of siliciclastic sedimentary rocks has been widely used to identify source rocks from which the investigated sedimentary rocks were derived (e.g., Armstrong-Altrin et al. 2004, 2012; Cullers 1995; Zaid 2012, 2013). Several major- and trace element-based discrimination diagrams have been proposed to infer the source/provenance of siliclastic rocks (e.g., Roser and Korsch 1988; Floyd et al. 1989; McLennan et al. 1980). On the provenance discrimination diagram of Roser and Korsch (1988), the Dakhla Shales plot in the fields of intermediate igneous and quartzose sedimentary with subordinate mafic igneous provenance (Fig. 11).

On the Al_2O_3–(CaO + Na_2O + K_2O)–(FeO^T + MgO) ternary diagram (Hayashi et al. 1997), the shales plot near the smectite field away from (FeO^T + MgO) apex and trend toward the Al_2O_3 apex (Fig. 12a). The plots of the shales on this diagram reiterates (albeit indirectly) the felsic nature of the source rocks. The concentration of zircon (Zr) is also used for characterizing the nature and composition of source rocks (Hayashi et al. 1997). As the average concentrations of Zr and Ti do not show a significantly wide variation (Table 3), it may be possible that significant fractionation of Zr and Ti might not have occurred during transportation and deposition of Dakhla Shales. The average zircon content of the Dakhla Shales varies from 38 to 173 ppm (Table 3), which is similar to the average value for granite and granodiorite. The TiO_2 versus Zr plot (Hayashi et al. 1997) of the Dakhla Shales represents predominantly felsic and intermediate igneous source rocks (Fig. 12b). The TiO_2/Zr plot thus suggests that the source area for shale from Quseir area (Gebel Atshan) was dominated by felsic rocks, whereas a partial contribution from mafic terrigenous is evident for shale from the Qena area (Gebel Abu Had

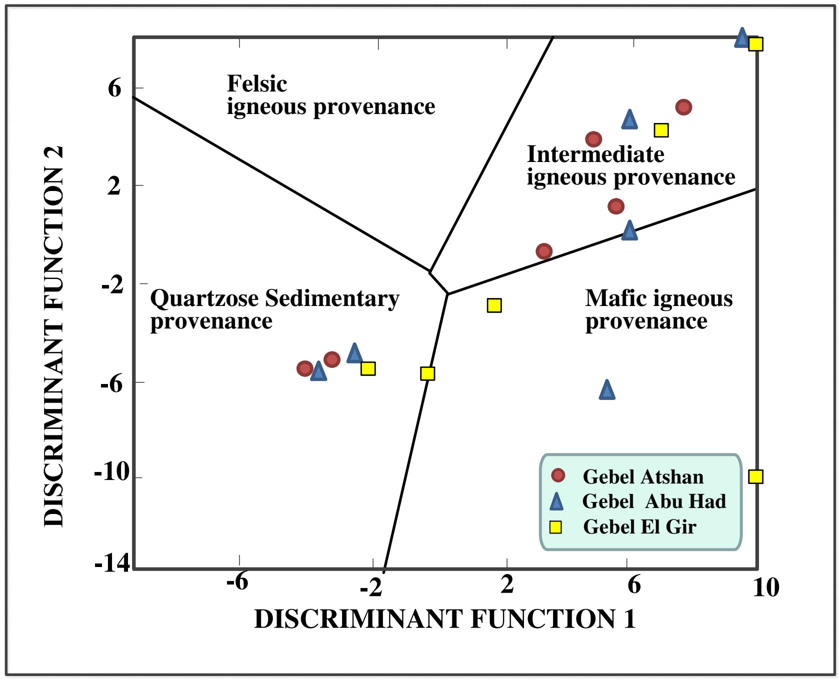

Fig. 11 Provenance discrimination diagram for shales (after Roser and Korsch 1988). Discriminant function 1=(−1.773×TiO_2%)+(0.607×Al_2O_3%)+(0.76×$Fe_2O_3^T$%)+(−1.5×MgO%)+(0.616×CaO%)+(0.509×Na_2O%)+(−1.22×K_2O%)+(−9.09). Discriminant function 2=(0.445×TiO_2%)+(0.07×Al2O3%)+(−0.25×$Fe_2O_3^T$%)+(−1.142×MgO%)+(0.438×CaO%)+(0.432×Na_2O%)+(1.426×K_2O%)+(−6.861)

and Gebel El Gir). Therefore, the different discrimination diagrams together indicate felsic and intermediate igneous source rocks of the Dakhla Shale.

Tectonic setting

Tectonic setting discrimination diagrams proposed by Bhatia (1983) and Roser and Korsch (1986) have been extensively used in sedimentary geochemistry studies to identify the tectonic setting of unknown sedimentary basins (Purevjav and Roser 2012; Yan et al. 2012). Tectonic provenances of ancient siliclastic rocks can be inferred from major- and trace-based discrimination diagrams proposed by several authors (e.g., Maynard et al. 1982; Bhatia 1983; Bhatia and Crook 1986; Roser and Korsch 1986). These diagrams classify the provenances into three or four categories on the basis of bulk geochemistry contrasts (e.g., oceanic island arc, continental island arc, active continental margin, passive margin; Bhatia and Crook 1986). On the bivariate discriminant function diagrams of Roser and Korsch (1986) and Bhatia (1983), the most studied shale samples plot in the active continental margin field with a few in the passive margin field (Fig. 13a, b). In active continental margin settings, sediments are deposited at subduction arc basins, strike-slip margins, and in proximal portions in back-arc basins (Alvarez and Roser 2007).

Numerous diagrams were available to identify the tectonic setting of a source region (Bhatia 1983; Roser and Korsch 1986) and are continuously used in many studies. Also, these diagrams were evaluated by other researchers and they cautioned the use of these previously proposed discrimination diagrams (e.g., Armstrong-Altrin and Verma 2005; Ryan and Williams 2007; Armstrong-Altrin 2014; Armstrong-Altrin et al. 2014). Recently, Verma and Armstrong-Altrin (2013) proposed two new discriminant function-based major element diagrams for the tectonic discrimination of siliciclastic sediments from three main tectonic settings: island or continental arc, continental rift, and collision, which have been created for the tectonic discrimination of high-silica [$(SiO_2)_{adj}$=63–95 %] and low-silica rocks [$(SiO_2)_{adj}$=35–63 %]. These two new diagrams were constructed based on worldwide examples of Neogene–Quaternary siliciclastic sediments from known tectonic settings, $\log_e$ ratio transformation of ten major elements with SiO_2 as the common denominator, and linear discriminant analysis of the $\log_e$-transformed ratio data. Recently, these diagrams were evaluated by Armstrong-Altrin (2014) and identified a good functioning of these diagrams for discriminating the tectonic setting of older sedimentary basins. Similarly, these diagrams were used in recent studies to discriminate the tectonic setting of a source region, based on sediment geochemistry (Armstrong-Altrin et al. 2014; Zaid and Gahtani 2015; Zaid 2015). On these plots (high-silica and low-silica diagrams; Fig. 14a, b), except two samples, the remaining samples plot in the rift field. The results obtained

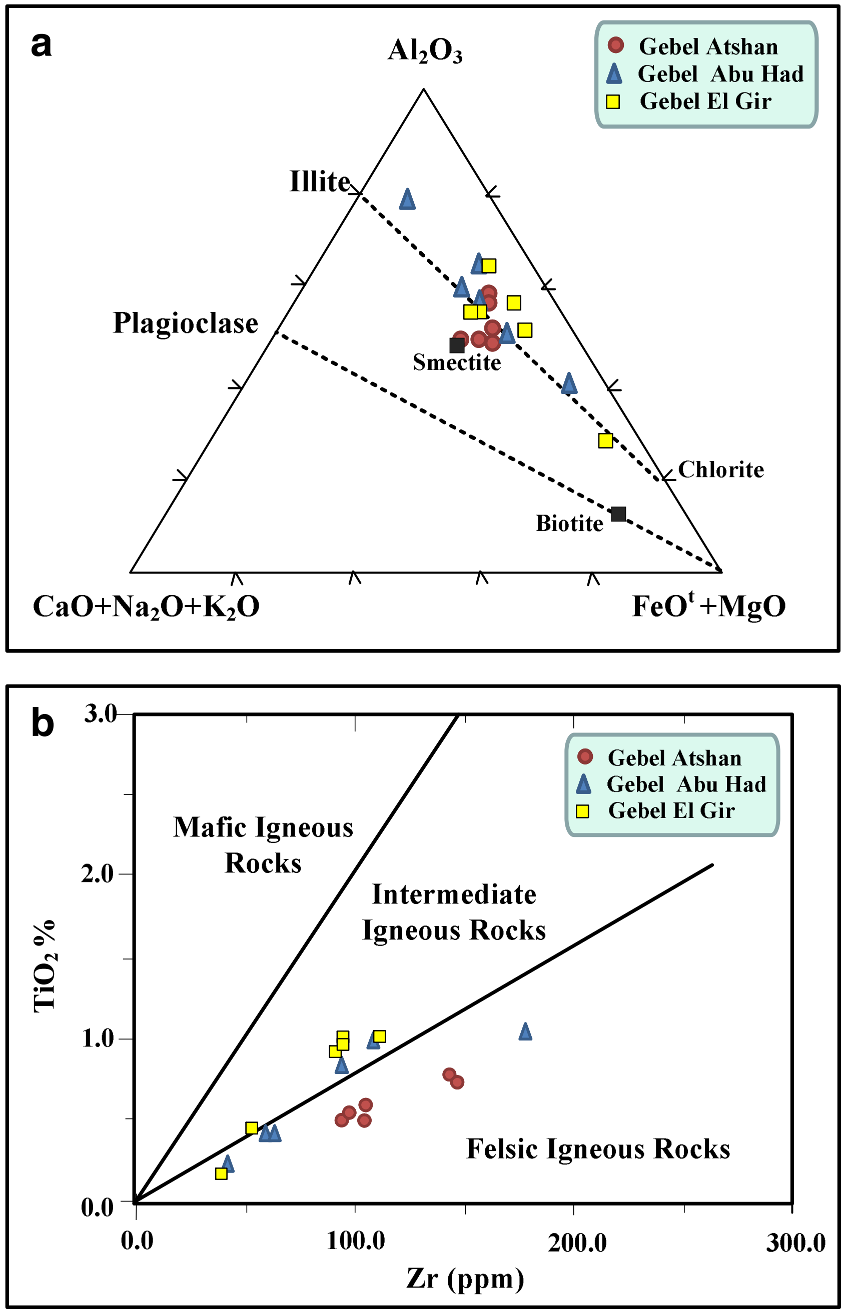

Fig. 12 Provenance diagrams. **a** Al_2O_3–(CaO + Na_2O + K_2O)–(FeO^T + MgO) ternary diagram (after Hayashi et al. 1997). **b** TiO_2 (wt%) versus Zr (ppm) bivariate diagram (after Hayashi et al. 1997)

from these two discriminant function-based multidimensional diagrams provide a good evidence for the Red Sea–Eastern Desert tectonic system, which is consistent with the general geology of Egypt (Said 1990).

In the present study, the studied shales plot in the semiarid field (Fig. 10). This was explained by Klitzsch (1990) who emphasized that during the Late Cretaceous and in connection with the Syrian arc development event, large parts of central and southern Egypt were uplifted and the sea retreated which led to changes in the environment of a large part of Egypt. According to Hendriks et al. (1987), it is believed that the main reasons for the genesis of the detrital clays of the Dakhla Shales were semiarid conditions which prevailed in source areas and the uplifting of large parts of Egypt. Due to the structural development of Egypt, the uplifted parts led to the development of soils in a large part of the studied area which led to the formation of smectite–kaolinite association in the studied Dakhla Shales as a result of alteration of micas and feldspar under semiarid conditions. The results of this study indicate that the Dakhla detrital clays were formed under semiarid conditions after the uplifting and changing in climate during the later part of the Cretaceous period.

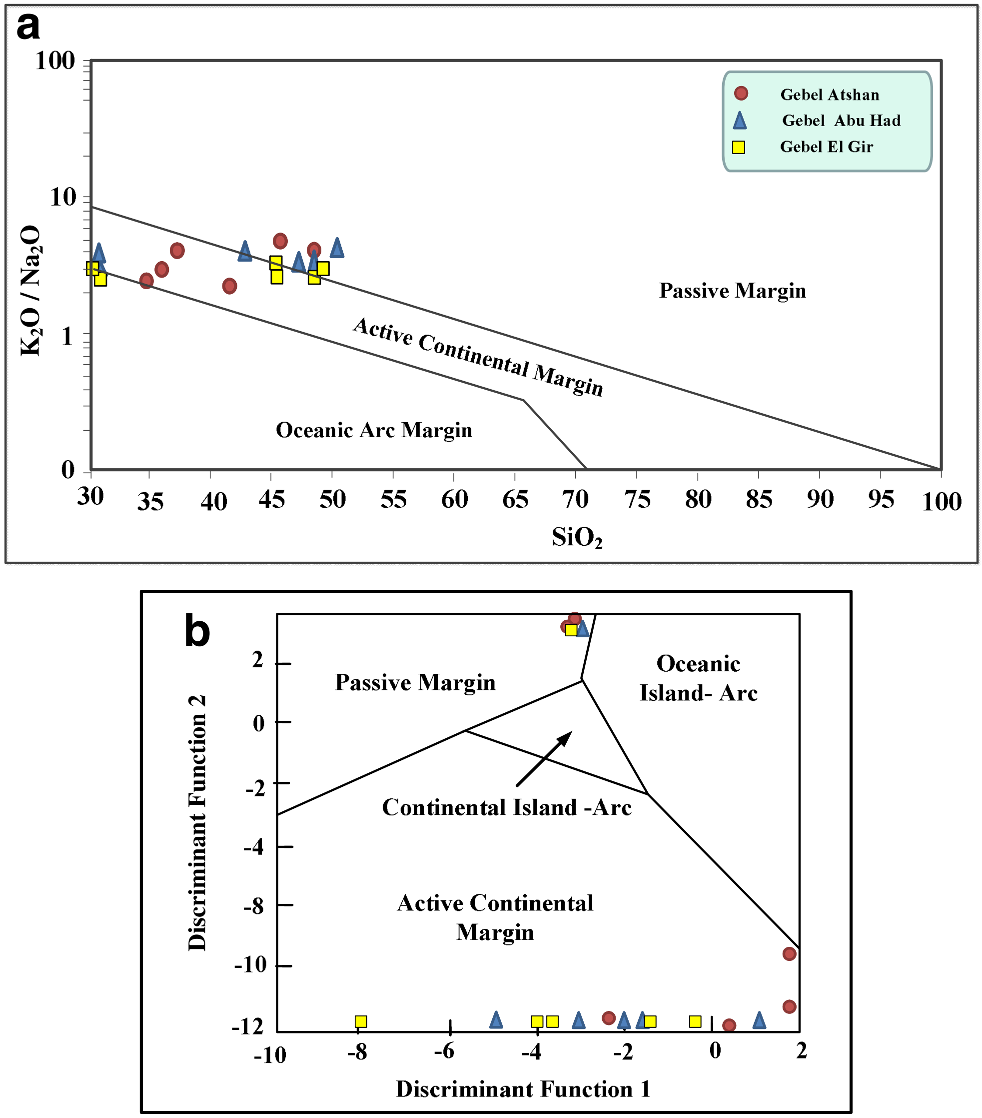

Fig. 13 Tectonic discrimination diagrams for the Dakhla Shales (fields are demarcated after **a** Roser and Korsch (1986), **b** Bhatia (1983))

Conclusions

The Dakhla Formation in the studied sections conformably overlies the Duwi Formation and unconformably underlies the Tarawan Chalk. This formation consists of a series of marls and shales and is subdivided into two members, namely Beida Shale Member at the top and Hamama Marl Member at the base. The Dakhla Shales are texturally classified as mudstones. Mineralogically, these shales consist mainly of smectite and kaolinite. The bulk rock mineralogy indicates the presence of phyllosilicates with abundant quartz and calcite and the common occurrence of anhydrite and a few and locally low dolomite, iron oxides, phosphate, feldspars, and gypsum contents. The average K_2O/Na_2O ratio is found higher in the Dakhla Shales in comparison to the NASC and PAAS. However, SiO_2/Al_2O_3 ratios among Dakhla Shales show close variations.

Depletion of Na_2O in the shales relative to PAAS suggests a lesser amount of plagioclase detritus in the shales. Depletion of TiO_2 and K_2O indicates the presence of relatively lesser quantities of phyllosilicates minerals in the shales and suggests felsic to intermediate igneous source rocks. ICV values of the Dakhla Shales indicate enrichment in rock-forming minerals in comparison with clays.

The Dakhla Shales have a moderate range in CIA values (71–87), indicating mature sediments, which is consistent with the SiO_2/Al_2O_3 ratios. The CIA, PIA, and CIW values (ranging from 81 to 93 %) indicate moderate to intense weathering in the source area. The Th/Sc–Zr/Sc diagram indicates a high influence of sediment recycling and mineral sorting.

The TiO_2 versus Zr plot (Hayashi et al. 1997) of the Dakhla Shales represents predominantly felsic and intermediate igneous source rocks. The recent tectonic discriminant function diagrams indicate a rift setting for the studied shales. The inferred tectonic setting for the Late Cretaceous–Early

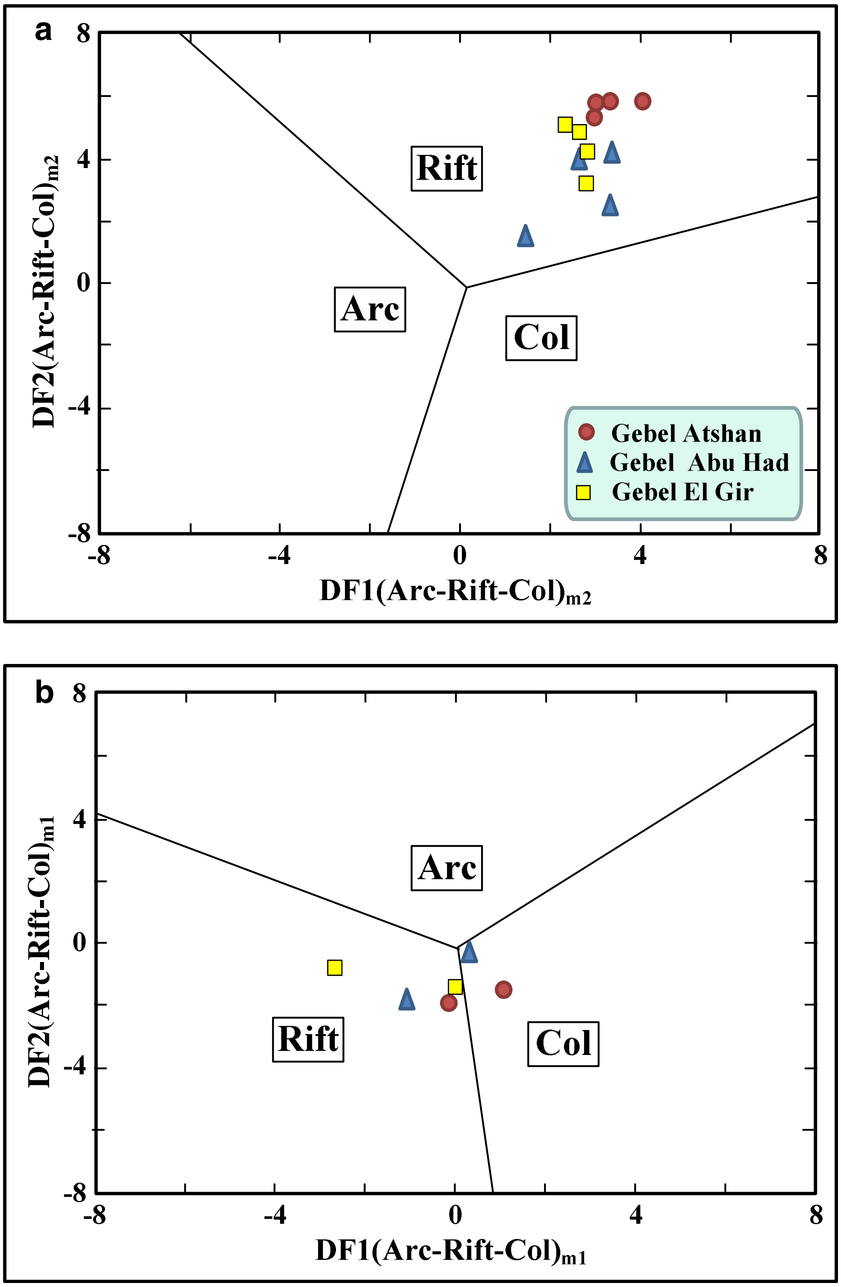

Fig. 14 **a** New discriminant function multidimensional diagram proposed by Verma and Armstrong-Altrin (2013) for high-silica clastic sediments from three tectonic settings (arc, continental rift, and collision). The subscript $_{m1}$ in DF1 and DF2 represents the high-silica diagram based on $\log_e$ ratios of major elements. The discriminant function equations are as follows: $DF1_{(Arc\text{-}Rift\text{-}Col)m1} = (-0.263 \times In(TiO_2/SiO_2)_{adj}) + (0.604 \times In(Al_2O_3/SiO_2)_{adj}) + (-1.725 \times In(Fe_2O_3{}^t/SiO_2)_{adj}) + (0.660 \times In(MnO/SiO_2)_{adj}) + (2.191 \times In(MgO/SiO_2)_{adj}) + (0.144 \times In(CaO/SiO_2)_{adj}) + (-1.304 \times In(Na_2O/SiO_2)_{adj}) + (0.054 \times In(K_2O/SiO_2)_{adj}) + (-0.330 \times In(P_2O_5/SiO_2)_{adj}) + 1.588$. $DF2_{(Arc\text{-}Rift\text{-}Col)m1} = (-1.196 \times In(TiO_2/SiO_2)_{adj}) + (1.604 \times In(Al_2O_3/SiO_2)_{adj}) + (0.303 \times In(Fe_2O_3{}^t/SiO_2)_{adj}) + (0.436 \times In(MnO/SiO_2)_{adj}) + (0.838 \times In(MgO/SiO_2)_{adj}) + (-0.407 \times In(CaO/SiO_2)_{adj}) + (1.021 \times In(Na_2O/SiO_2)_{adj}) + (-1.706 \times In(K_2O/SiO_2)_{adj}) + (-0.126 \times In(P_2O_5/SiO_2)_{adj}) - 1.068$. **b** New discriminant function multidimensional diagram proposed by Verma and Armstrong-Altrin (2013) for low-silica clastic sediments from three tectonic settings (arc, continental rift, and collision). The subscript $_{m2}$ in DF1 and DF2 represents the low-silica diagram based on $\log_e$ ratio of major elements. Discriminant function equations are as follows: $DF1_{(Arc\text{-}Rift\text{-}Col)m2} = (0.608 \times In(TiO_2/SiO_2)_{adj}) + (-1.854 \times In\ (Al_2O_3/SiO_2)_{adj}) + (0.299 \times In(Fe_2O_3{}^t/SiO_2)_{adj}) + (-0.550 \times In(MnO/SiO_2)_{adj}) + (0.120 \times In(MgO/SiO_2)_{adj}) + (0.194 \times In(CaO/SiO_2)_{adj}) + (-1.510 \times In(Na_2O/SiO_2)_{adj}) + (1.941 \times In(K_2O/SiO_2)_{adj}) + (0.003 \times In(P_2O_5/SiO_2)_{adj}) - 0.294$. $DF2_{(Arc\text{-}Rift\text{-}Col)m1} = (-0.554 \times In(TiO_2/SiO_2)_{adj}) + (-0.995 \times In\ (Al_2O_3/SiO_2)_{adj}) + (1.765 \times In(Fe_2O_3{}^t/SiO_2)_{adj}) + (-1.391 \times In(MnO/SiO_2)_{adj}) + (-1.034 \times In(MgO/SiO_2)_{adj}) + (0.225 \times In(CaO/SiO_2)_{adj}) + (0.713 \times In(Na_2O/SiO_2)_{adj}) + (0.330 \times In(K_2O/SiO_2)_{adj}) + (0.637 \times In(P_2O_5/SiO_2)_{adj}) - 3.631$

Tertiary Dakhla Shales in Quseir–Qena Province, central Egypt, is in agreement with the tectonic evolutionary history of the central Egypt during the Late Cretaceous–Early Tertiary.

Acknowledgments The author acknowledges the journal reviewers for their very constructive and helpful comments as well as for editorial comments by A. Al-Amri, which helped to improve the manuscript.

References

Abdel Razik TM (1972) Comparative studies on the Upper Cretaceous Early Paleocene sediments on the Red Sea Coast, Nile Valley and Western Desert, 8th Arab Petrol Cong Algiers Paper 71 (B-3), 23 pp

Ahmed HA (1997) Mineralogical and geochemical studies of the black shales intercalated with phosphorite deposits at Abu Tartur area Western Desert, Egypt. M.Sc. thesis, Ain Shams Uni Cairo, Egypt, 284p

Alvarez NO, Roser BP (2007) Geochemistry of black shales from the Lower Cretaceous Paja Formation, Eastern Cordillera, Colombia: source weathering, provenance and tectonic setting. J South Am Earth Sci 23(4):271–289

Armstrong-Altrin JS (2009) Provenance of sands from Cazones, Acapulco, and Bahía Kino beaches, Mexico. Rev Mex Cienc Geol 26(3):764–782

Armstrong-Altrin JS (2014) Evaluation of two multidimensional discrimination diagrams from beach and deep-sea sediments from the Gulf of Mexico and their application to Precambrian clastic sedimentary rocks. Int Geol Rev. doi:10.1080/00206814.2014.936055

Armstrong-Altrin JS, Verma SP (2005) Critical evaluation of six tectonic setting discrimination diagrams using geochemical data of Neogene sediments from known tectonic setting. Sediment Geol 177:115–129

Armstrong-Altrin JS, Lee YI, Verma SP, Ramasamy S (2004) Geochemistry of sandstones from the Upper Miocene Kudankulam Formation, southern India: implications for provenance, weathering, and tectonic setting. J Sediment Res 74:285–297

Armstrong-Altrin JS, Lee YI, Kasper-Zubillaga JJ, Carranza-Edwards A, Garcia D, Eby N, Balaram V, Cruz-Ortiz NL (2012) Geochemistry of beach sands along the western Gulf of Mexico, Mexico: implication for provenance. Chem Erde Geochem 72:345–362

Armstrong-Altrin JS, Nagarajan R, Madhavaraju J, Rosalez-Hoz L, Lee YI, Balaram V, Cruz-Martínez A, Avila-Ramírez G (2013) Geochemistry of the Jurassic and Upper Cretaceous shales from the Molango Region, Hidalgo, eastern Mexico: implications for source-area weathering, provenance, and tectonic setting. C R Geosci 345:185–202

Armstrong-Altrin JS, Nagarajan R, Lee YI, Kasper-Zubillaga JJ, Córdoba-Saldaña LP (2014) Geochemistry of sands along the San Nicolás and San Carlos beaches, Gulf of California, Mexico: implication for provenance. Turk J Earth Sci 23:533–558

Armstrong-Altrin JS, Machain-Castillo ML, Rosales-Hoz L, Carranza-Edwards A, Sanchez-Cabeza JA, Ruíz-Fernández AC (2015) Geochemistry of deep sea sediments from the south-western Gulf of Mexico, Mexico: implication for depositional environment. Cont Shelf Res. doi:10.1016/j.csr.2015.01.003

Awad GH, Ghobrial MG (1965) Zonal stratigraphy of the Kharga Oasis. Geol Surv Egypt 34:77

Bhatia MR (1983) Plate tectonics and geochemical composition of sandstones. J Geol 91:611–627

Bhatia MR (1985) Rare earth element geochemistry of Australian Paleozoic graywackes and mudrocks: provenance and tectonic control. Sediment Geol 45:97–113

Bhatia MR, Crook KAW (1986) Trace element characteristics of graywackes and tectonic setting discrimination of sedimentary basins. Contrib Mineral Petrol 92:181–193

Blatt H (1985) Provenance studies and mudrocks. J Sediment Petrol 55: 69–75

Chamley H (1989) Clay sedimentology. Springer, Berlin, 623 pp

Condie KC (1993) Chemical composition and evolution of the upper continental crust: contrasting results from surface samples and shales. Chem Geol 104:1–37

Condie KC, Boryta MD, Liu J, Quian X (1992) The origin of khondalites: geochemical evidence from the Archean to early Proterozoic granulite belt in the North China craton. Precam Res 59:207–223

Cox R, Lower DR, Cullers RL (1995) The influence of sediment recycling and basement composition on evolution of mudrock chemistry in the southwestern United States. Geochim Cosmochim Acta 59:2919–2940

Cullers RL (1995) The controls on the major- and trace-element evolution of shales, siltstones and sandstones of Ordovician to Tertiary age in the West Mountains region, Colorado, U. S. A. Chem Geol 123: 107–131

Cullers RL (2000) The geochemistry of shales, siltstones and sandstones of Pennsylvanian–Permian age, Colorado, USA: implications for provenance and metamorphic studies. Lithos 51:181–203

Davis JC (1986) Statistics and data analysis in geology. Wiley, p 646

Deepthi K, Natesan U, Muthulakshmi AL, Ferrer VA, Venugopalan VP, Narasimhan SV (2012) Geochemical characteristics and depositional environment of Kalpakkam, Southeast coast of India. Environ. Earth Sci

Deru X, Xuexang G, Pengehun L, Guanghao C, Bin X, Bachinski R, Zhuanli H, Gonggu F (2007) Mesoproterozoic–Neoproterozoic transition: geochemistry, provenance and tectonic setting of clastic sedimentary rocks on the SE margin of the Yangtze Block, South China. J Asian Earth Sci 29:637–650

El-Hawat AS (1997) Sedimentary basins of Egypt: an overview of dynamic stratigraphy. In: SeJley RC (ed) African basins, sedimentary basins of the world, 3. Amsterdam, Elsevier, pp 39–85

El-Azabi MH, Farouk S (2010) High resolution sequence stratigraphy of the Maastrichtian–Ypresian succession along the eastern scarp face of Kharga Oasis, southern Western Desert, Egypt. Sedimentology, 1–35

El-Dahhar MA (1987) Diagenetic pyrite framboids in the phosphate deposits of Abu Tartur area, Western Desert, Egypt. J Afr Earth Sci 6: 807–811

Faris M (1984) The Cretaceous/Tertiary boundary in Central Egypt (Duwi region, Nile Valley, Kharga and Dakhla Oasis). N Jb Geol Paläont (Monatsh) Stuttgart 7:385–392

Faris M, Strougo A (1998) The lower Libyan of Farafra (Western Desert) and Luxor (Nile Valley): correlation by calcerous nannofossils. Middle East Research Center, Ain Shams Univ. Earth Sci Ser 12: 137–156

Faris M, Abd El-Hameed AT, Marzouk AM, Ghandour LM (1999) Early Paleogene calcareous nannofossil and planktonic foraminiferal biostratigraphy in Central Egypt. N Jb Geol Paläont (Abh) 213–2:261–288

Fedo CM, Nesbitt HW, Young GM (1995) Unraveling the effects of Kmetasomatism in sedimentary rocks and paleosols with implications for palaeoweathering conditions and provenance. Geology 23: 921–924

Fedo CM, Eriksson KA, Krogstad EJ (1996) Geochemistry of shales from the Archean (~3.0 Ga) Buhwa Greenstone Belt, Zimbabwe: implications for provenance and source-area weathering. Geochim Cosmochim Acta 60:1751–1763

Floyd PA, Franke W, Shail R, Dorr W (1989) Geochemistry and tectonic setting of Lewisian clastic metasediments from the Early Proterozoic Loch Maree Group of Gairloch, NW Scotland. Precam Res 45:203–214

Fyffe LR, Pickerill RK (1993) Geochemistry of Upper Cambrian-Lower Ordovician black shale along a northeastern Appalachian transect. Geol Soc Am Bull 105:896–910

Germann K, Bock WD, Ganz H, Schröter T, Tröger U (1987) Depositional conditions of Late Cretaceous phosphorites and black-shales in Egypt. Berl Geowiss Abh A 75(3):629–668

Ghandour IM, Harue M, Wataru M (2003) Mineralogical and chemical characteristics of Bajocian-Bathonian shales, G. Al-Maghara, North Sinai, Egypt: climatic and environmental significance. Geochem J 37:87–108

Ghosh S, Sarkar S, Ghosh P (2012) Petrography and major element geochemistry of the Permo-Triassic sandstones, central India: implications for provenance in an intracratonic pull-apart basin. J Asian Earth Sci 43:207–240

Gindy AR (1983) Factors controlling the clay mineralogy of Egyptian Phanerozoic mudrocks and marls. Geol Jb B 49:3–25, Hannover

Graver JI, Scott TJ (1995) Trace elements in shale as indicators of crustal provenance and terrain accretion of the southern Canadian cordillera. Geol Soc Am Bull 107:440–453

Gromet LP, Dymek RF, Haskin LA, Korotev RL (1984) The North American Shale Composite: its compilations, major and trace element characteristics. Geochim Cosmochim Acta 48:2469–2482

Hallam A, Grose JA, Ruffell AH (1991) Paleoclimatic significance of changes in clay mineralogy across the Jurassic-Cretaceous boundary in England and France. Palaeogeogr Palaeoclimatol Palaeoecol 81: 173–187

Hardy R, Tucker M (1988) X-ray powder diffraction of sediments. In: Tucker M (ed) Techniques in sedimentology. Cambridge, Blackwell, pp 191–228

Harnois L (1988) The CIW index: a new chemical index of weathering. Sed Geol 55:319–322

Hayashi KI, Fujisawa H, Holland HD, Ohomoto H (1997) Geochemistry of ~1.9 Ga sedimentary rocks from northern Labrador, Canada. Geochim Cosmochim Acta 61(19):4115–4137

Hendriks F (1985) Upper Cretaceous to lower Tertiary sedimentary environments and clay mineral associations in the Kharga Oasis area, Egypt. N Jb Geol Paläont Mh 10:579–591

Hendriks F (1988) Die Kreide und das Alttertiar in Südostägypten: Sedimentologie und Tonmineralogie eines intrakratonalen Ablagerungsraumes. Berl Geowiss Abh A 104:129, Berlin

Hendriks F, Luger P, Bowitz J, Kallenback H (1987) Evolution of depositional environments of SE-Egypt during the Cretaceous and Lower Tertiary. Berl Geowiss Abh A 75:49–82, Berlin

Hendriks F, Luger P, Strouhal A (1990) Early tertiary marine palygorskite and sepiolite neoformation in SE Egypt. Z Deut Geol Ges 141:87–97

Herron MM (1988) Geochemical classification of terrigenous sands and shales from core or log data. J Sediment Petrol 58:820–829

Ismael SI (1996) Mineralogical and geochemical studies of the black shales intercalated with the phosphate deposits along the Red Sea coast, Egypt. Ph.D. thesis. Ain Shams Uni Cairo, Egypt.

Issawi B (1972) Review of Upper Cretaceous-Lower Tertiary stratigraphy in Central and Southern Egypt. Am Assoc Pet Geol Bull 56:1448–1463

Jafarzadeh M, Hosseini-Barzi M (2008) Petrography and geochemistry of Ahwaz sandstone member of Asmari Formation, Zagros, Iran: implications on provenance and tectonic setting. Rev Mex Cienc Geol 25(2):247–260

Kampunzu AB, Cailteux JLH, Moine B, Loris HNBT (2005) Geochemical characterization, provenance, source and depositional environment of 'Roches Argilo-Talqueuses' (TAR) and Mines Subgroups sedimentary rocks in the Neoproterozoic Katangan Belt (Congo): lithostratigraphic implications. J Afr Earth Sci 42:119–133

Klitzsch E (1990) The Paleozoic. In: Said R (ed) The geology of Egypt. A.A. Balkema, Rotterdam, pp 393–406

Long X, Yuan C, Sun M, Xiao W, Wang Y, Cai K, Jiang Y (2012) Geochemistry and Nd isotopic composition of the Early Paleozoic flysch sequence in the Chinese Altai, central Asia: evidence for a northward-derived mafic source and insight into Nd model ages in accretionary orogen. Gondwana Res 22:554–566

Maynard JB, Valloni R, Yu HS (1982) Composition of modern deep-sea sands from arc-related basins, vol. 10. Geol Soc London Spec Publ pp 551–561

McCann T (1991) Petrological and geochemical determination of provenance in the southern Welsh Basin. In: Morton AC, Todd SP, Haughton PDW (eds) Developments in sedimentary provenance studies, vol. 57. Geol Soc London Spec Publ, pp 215–230

McLennan SM (1993) Weathering and global denudation. J Geol 101: 295–303

McLennan SM, Nance WB, Taylor SR (1980) Rare earth element-thorium correlation in sedimentary rocks and the composition of the continental crust. Geochim Cosmochim Acta 44:1833–1839

McLennan SM, Hemming S, Mcdaniel DK, Hanson GN (1993) Geochemical approaches to sedimentation, provenance and tectonics. In: Johnsson JM, Basu A (eds) Processes controlling the composition of clastic sediments. Geol Soc Am Spec Pap 284:21–40

Millot G (1970) Geology of clays. Springer, Heidelberg, 429 p

Moore DM, Reynolds RC Jr (1997) X-ray diffraction and the identification and analysis of clay minerals. Oxford University Press, New York, 378 pp

Moosavirad SM, Janardhana MR, Sethumadhav MS, Moghadam MR, Shankara M (2011) Geochemistry of lower Jurassic shales of the Shemshak Formation, Kerman Province, Central Iran: provenance, source weathering and tectonic setting. Chem Erde 71:279–288

Nagarajan R, Madhavaraju J, Nagendra R, Armstrong-Altrin JS, Moutte J (2007) Geochemistry of Neoproterozoic shales of the Rabanpalli formation, Bhima Basin, northern Karnataka, southern India: implications for provenance and paleoredox conditions. Rev Mex Cienc Geol 24(2):150–160

Nesbitt HW, Young GM (1982) Early Proterozoic climates and plate motions inferred from major element chemistry of lutites. Nature 299:715–717

Nesbitt HW, Young GM (1984) Prediction of some weathering trends of plutonic and volcanic rocks based on thermodynamic and kinetic considerations. Geochim Cosmochim Acta 48:1523–1534

Nesbitt HW, Young GM (1989) Formation and diagenesis of weathering profiles. J Geol 97:129–147

Nesbitt HW, Markovics G, Price RC (1980) Chemical processes affecting alkalies and alkaline earths during continental weathering. Geochim Cosmochim Acta 44:1695–1766, London

Nesbitt HW, Fedo CM, Young GM (1997) Quartz and feldspar stability, steady and non-steady-state weathering, and petrogenesis of siliciclastic sands and muds. J Geol 105:173–191

Obaidalla NA, Hewaidy AA, Hosny AM, Mahfouz KH (2008) The Paleocene/Eocene transition at Kharga Oasis, Western Desert, Egypt: litho-biostratigraphy and paleoenvironment, 8th Ann Meet Paleontol Soc, Cairo, Abstracts, pp. 7–8

Ollier CD, Galloway RW (1990) The laterite profile ferricrete and unconformity. Canda Verlag, Cremlingen 17:97–109

Pettijohn FJ (1975) Sedimentary rocks, 3rd edn. Harper and Row, New York, 628 p

Prevot L, El Faleh EM, Lucas J (1989) Details on synthetic apatites formed through bacterial mediation: mineralogy and chemistry of the products. In: Lucas J, Cook PJ, Prevot L (eds) Apatite and phosphorites. Sci Geol Bull Strasbourg 42:237–254

Purevjav N, Roser B (2012) Geochemistry of Devonian-Carboniferous clastic sediments of the Tsetserleg terrane, Hangay Basin, central Mongolia: provenance, source weathering, and tectonic setting. Island Arc 21:270–287

Roser BP, Korsch RJ (1986) Determination of tectonic setting of sandstone-mudstone suites using SiO_2 content and K_2O/Na_2O ratio. J Geol 94(5):635–650

Roser BP, Korsch RJ (1988) Provenance signatures of sandstone-mudstone suites determined using discriminant function analysis of major-element data. Chem Geol 67:119–139

Ryan KM, Williams DM (2007) Testing the reliability of discrimination diagrams for determining the tectonic depositional environment of ancient sedimentary basins. Chem Geol 242:103–125

Said R (1960) Planktonic foraminifera from the Thebes Formation Luxor, Egypt. Micropaleontology 6:277–286

Said R (1961) Tectonic frame work of Egypt and its influence on the distribution of foraminifera. Am Assoc Pet Geol Bull 45:198–218

Said R (1962) The geology of Egypt. Elsevier, New York, 377 p

Said R (1990) The geology of Egypt. A.A. Balkema, Rotterdam, 734p

Said R (1992) The geology of Egypt. Elsevier, Rotterdam

Schieber J, Baird G (2001) On the origin and significance of pyrite spheres in Devonian black shale of North America. J Sediment Res 71(1):155–166

Selley RC (1988) Applied sedimentology. Textbook. p 446

Selvaraj K, Chen CTA (2006) Moderate chemical weathering of subtropical Taiwan: constraints from solid-phase geochemistry of sediments and sedimentary rocks. J Geol 14:101–116

Sugitani K, Horiuchi Y, Adachi M, Sugisaki R (1996) Anomalously low Al2O3/TiO2 values for Archean cherts from the Pilbara Block, Western Australia: possible evidence for extensive chemical weathering on the early earth. Precam Res 80:49–76

Surdam RC, Stanley KO (1979) Lacustrine sedimentation during the culminating phase of Eocene Lake Gosiute, Wyoming (Green River Formation). Geol Soc Am Bull 90:93–110

Suttner LJ, Dutta PK (1986) Alluvial sandstone composition and palaeoclimate. 1. Framework mineralogy. J Sediment Petrol 56(3): 329–345

Tantawy AA, Keller G, Adatte T, Stinnesbeck W, Kassab A, Schulte P (2001) Maastrichtian to Paleocene depositional environment of the Dakhla Formation, Western Desert, Egypt: sedimentology, mineralogy and integrated micro- and macrofossil biostratigraphies. Cretac Res 22:795

Taylor SR, McLennan SM (1985) The continental crust: its composition and evolution. Blackwell, Oxford, 312 p

Thiry M, Jaquin T (1993) Clay mineral distribution related to rift activity, sea-level changes and paleoceanography in the Cretaceous of the Atlantic Ocean. Clay Miner 28:61–84

Turekian KK, Wedepohl KH (1961) Distribution of the elements in some major units of the earth's crust. Bull Geol Soc Am 72:175–192

Verma SP, Armstrong-Altrin JS (2013) New multi-dimensional diagrams for tectonic discrimination of siliciclastic sediments and their application to Precambrian basins. Chem Geol 355:117–180

Vine JD, Tourtelot EB (1970) Geochemistry of black shales—a summary report. Econ Geol 65:253–273

Yan Z, Wang Z, Yan Q, Wang T, Guo X (2012) Geochemical constraints on the provenance and depositional setting of the Devonian Liuling Group, East Qinling mountains, central China: implications for the tectonic evolution of the Qinling Orogenic Belt. J Sediment Res 82: 9–24

Zaid SM (2012) Provenance, diagenesis, tectonic setting and geochemistry of Rudies sandstone (Lower Miocene), Warda Field, Gulf of Suez, Egypt. J Afr Earth Sci 66–7:56–71

Zaid SM (2013) Provenance, diagenesis, tectonic setting and reservoir quality of the sandstones of the Kareem Formation, Gulf of Suez, Egypt. J Afr Earth Sci 85:31–52

Zaid SM (2015) Geochemistry of sandstones from the Pliocene Gabir Formation, north Marsa Alam, Red Sea, Egypt: implication for provenance, weathering and tectonic setting. J Afr Earth Sci 102: 1–17

Zaid SM, Gahtani FA (2015) Provenance, diagenesis, tectonic setting and geochemistry of Hawkesbury sandstone (Middle Triassic), southern Sydney Basin, Australia. Turk J Earth Sci 24:72–98

Zittel AK (1883) Beitrage zur Geologie und Palaontologie der Libyschen Wuste und der angrenzenden Gebiete von Aegypten. Palaeontographica 30, 3.F., 1, 147, 2, p 237